Interfacial and Bulk Properties of Vapor-Liquid Equilibria in the System Toluene + Hydrogen Chloride + Carbon Dioxide by Molecular Simulation and Density Gradient Theory + PC-SAFT

Stephan Werth[a], Maximilian Kohns[a], Kai Langenbach[1,a], Manfred Heilig[b],
Martin Horsch[a], Hans Hasse[a]

[a] *University of Kaiserslautern, Laboratory of Engineering Thermodynamics,*
Erwin-Schrödinger Str. 44, D-67663 Kaiserslautern, Germany
[b] *GCP Chemical and Process Engineering, BASF SE, D-67056 Ludwigshafen, Germany*

Abstract

Interfacial and bulk properties of vapor-liquid equilibria (VLE) in systems containing toluene, hydrogen chloride (HCl), and carbon dioxide (CO_2) are studied by molecular dynamics simulations and density gradient theory + PC-SAFT. The pure components, the three binary mixtures, and the ternary mixture are studied systematically. A new PC-SAFT model of HCl is developed and mixture models are adjusted to binary VLE data. The focus of the studies is on the temperatures 333 and 353 K for which both HCl and CO_2 are supercritical. The simulation results are compared to experimental data, where such data are available. VLE bulk properties are well described. For

---

[1] Corresponding author; kai.langenbach@mv.uni-kl.de; phone: +49-631 / 205-2176; fax: +49-631 / 205-3835.

the interfacial tension, only pure component data are available, which are well predicted. For the mixtures, data on the interfacial tension are predicted. A strong adsorption of both HCl and CO_2 at the vapor-liquid interface is found from both methods.

Keywords: Interfacial tension, Interfacial adsorption, Molecular dynamics, Density gradient theory, PC-SAFT

---

1. Introduction

Interfacial properties of the vapor-liquid equilibrium are important for many applications in process engineering, including separations like absorption but also multi-phase reactions. They are especially important for phenomena like nucleation and foaming. Experimental data on interfacial properties of mixtures are in most cases limited to the interfacial tension and even such data are rarely available. Hence, it is desirable to have models which enable predicting and analyzing interfacial properties. The most attractive methods are molecular simulation based on force fields and density gradient theory coupled with an equation of state [1–8].

Both methods are used in the present work for studying interfacial properties of toluene, carbon dioxide (CO_2) and hydrogen chloride (HCl), and their mixtures. These three molecules differ significantly in structure and polarity.

HCl forms hydrogen bonds and is strongly dipolar, CO_2 is slightly larger and quadrupolar. Toluene is much larger and almost nonpolar. The system toluene + HCl + CO_2 can also be considered as a model system for similar mixtures, which are important in reaction engineering, where toluene stands for the solvent and HCl and CO_2 stand for reacting gases or gaseous products. The present study focuses on the temperature range 333 to 353 K where both HCl and CO_2 are supercritical and the binary vapor-liquid equilibria of toluene + HCl and toluene + CO_2 show wide-boiling behavior. There are many experimental studies on the VLE of toluene + CO_2 mixtures in the temperature range investigated in the present work [9–17]. The binary system CO_2 + HCl does not exhibit a VLE at temperatures in the range given above. A VLE is obtained in that system at 290 K, where it shows aceotropic behavior [18, 19]. An overview of the experimental data of the binary mixtures used in the present work is shown in Table 1.

[Table 1 about here.]

From a molecular point of view, at a vapor-liquid interface the density changes smoothly from its liquid bulk to its vapor bulk value. This transition from the vapor to the liquid phase along a coordinate normal to the interface can be described well by a hyperbolic tangent function for the density of a pure fluid [20–22]. For mixtures, however, complex phenomena are occasionally observed in that transition region [22–26]. This holds especially for wide-boiling mixtures [27–33]. While the density of such mixtures decreases monotonously from the bulk liquid to the bulk vapor, the densities of some of the individual components do not. Enrichment effects may occur, such that a maximum of the density of the light-boiling component is observed in the interfacial region, where it can reach values several times larger than its largest bulk value. Such interfacial enrichments in VLE of mixtures have been discussed in the literature [27–34], but no systematic evaluation of the phenomenon of interfacial enrichment has been conducted so far for complex systems like the ternary one studied in the present work. From the available VLE data, it can be deduced that high enrichments occur in mixtures of water and CO_2, where the component density of CO_2 is reported to be up to 7 times higher at the interface than in the bulk phases [33, 35–37]. In mixtures of water and alcohols [7], as well as DMF + alkanes [26], component densities were found which were up to 10 times higher than the highest corresponding component density in the bulk phase. Only small enrichments were found for mixtures of alkanes [24, 34], mixtures of poly(dimethylsiloxane) + acid gases [38], mixtures of carbon dioxide + sulfur dioxide, mixtures of carbon dioxide

+ hydrogen sulfide [39], mixtures of acetone + nitrogen and of acetone + oxygen [22].

In the present work, molecular dynamics (MD) simulations with the $ls1$ *mardyn* program [40] and calculations applying the density gradient theory coupled with the PC-SAFT equation of state are conducted to investigate the interfacial tension and the interfacial enrichment in multi-component systems. The force field models for the MD simulations are taken from previous work of our group [3, 41]. The PC-SAFT parameters for toluene and CO_2 are taken from Gross and Sadowski [4]. A new model for HCl is developed in the present work. The molecular model parameters of the pure components were adjusted to describe the saturated liquid density, vapor pressure and enthalpy of vaporization, which is well done [3, 41]. The molecular models for CO_2 and HCl were also evaluated with respect to transport properties. They show a very good agreement with experimental data for the self diffusion coefficient, shear viscosity and thermal conductivity [41, 42].

The interfacial tension is usually not taken into account in the parameterization of molecular models. Molecular models from previous work of our group were adjusted to reproduce the vapor pressure and the saturated liquid density [43, 44]. These models overestimate the interfacial tension by

20 % on average [45–48]. Similar findings were obtained for other molecular models which were parameterized with respect to bulk properties only [22, 27, 49–56]. Attempts to reconciliate the quality of the results for bulk and interfacial properties by including the latter into the fit of the parameters of the molecular models have so far not been successful [47, 57, 58]. Despite these shortcomings, the molecular models from the literature were used straightforwardly in the present work. No parameters were changed. Hence, all results from the MD simulations in the present work are predictions of interfacial properties from bulk properties.

While molecular simulation resolves thermodynamic properties on the scale of atoms and molecules, density gradient theory (DGT) takes a continuum perspective. It was first introduced by van der Waals [59] and then rediscovered by Cahn and Hilliard [60] for application to pure compounds. Later it was generalized for the description of mixtures by Poser and Sanchez [24]. In combination with a physically based equation of state, DGT can describe with good accuracy the interfacial tension of both pure compounds [6] and mixtures [7].

In the present work, bulk and interfacial properties from both MD simulation and DGT + PC-SAFT of pure components as well as of binary and ternary mixtures are reported. The binary and ternary mixtures of toluene with HCl and CO_2 are investigated in the temperatures range 333 and 353 K, while the mixtures of HCl and CO_2 are investigated at temperatures of 290 K. Bulk properties, i.e. saturated densities, vapor pressures, compositions and Henry's law constants, are reported for a wide range of compositions. Interfacial properties, i.e. the interfacial tension, interfacial enrichment and interfacial adsorption are investigated systematically. Comparisons with experimental data are given if such data is available.

2. Modelling and Simulation

2.1. Fundamentals

Thermodynamically, the interfacial tension γ is defined as the change in free energy upon a variation of the interfacial area

$$\gamma = \left(\frac{\partial A}{\partial S}\right)_{N,V,T}, \tag{1}$$

where A is the Helmholtz free energy and S is the interfacial area. For determination of the interfacial tension in molecular simulation several methods can be used, either mechanical routes [61–63], the test-area method [64, 65] or finite-size scaling based on grand-canonical sampling [66–70]. The mechanical route, which is used in the present work, can be realized straightforwardly based on the intermolecular virial [61–63], which is also used for the pressure calculation in MD simulation [61]. For planar interfaces, the thermodynamic and the mechanical route are equivalent. There are significant deviations for curved interfaces if the second order virial contributions are neglected in the application of the mechanical route [70–73].

Interfacial adsorption may lead to an enrichment of components of the studied mixture at interfaces between phases. To quantify this enrichment, the interfacial enrichment E_i of component i is introduced. It is defined in the present work as the ratio of the maximum of the local component density $\rho_i(y)$ in the interfacial region and of the highest density of the same component in the bulk phases

$$E_i = \frac{\max(\rho_i(y))}{\max(\rho'_i, \rho''_i)}. \tag{2}$$

Hereby, ρ'_i and ρ''_i are the bulk liquid and the bulk vapor density of component i, respectively, and y is a spatial coordinate perpendicular to the interface. In the present work, the highest bulk value of the component densities is always reached in the liquid phase.

The enrichment E_i is related to adsorption at the interface, but does not express the same information. Adsorption may occur even if there is no enrichment ($E_i = 1$), but enrichment will always result in adsorption. The relative adsorption is calculated under the assumption that the reference component j (which is toluene here) does not adsorb at the interface. On the basis of the density profiles of component i and j, $\rho_i(y)$ and $\rho_i(y)$, the relative adsorption defined by Gibbs [74] can be computed by the symmetric interface segregation according to Wadewitz and Winkelmann [23]

$$\Gamma_i^{(j)} = -\left(\rho_i^{'} - \rho_i^{''}\right) \int_{-\infty}^{\infty} \mathrm{d}y \left[\frac{\rho_j(y) - \rho_j^{'}}{\rho_j^{'} - \rho_j^{''}} - \frac{\rho_i(y) - \rho_i^{'}}{\rho_i^{'} - \rho_i^{''}}\right], \tag{3}$$

where $\rho_i^{'}$, $\rho_i^{''}$ and $\rho_j^{'}$, $\rho_j^{''}$ are the component densities of i and j in the two bulk phases $'$ and $''$.

2.2. Molecular Simulation

The molecular model for CO_2 is taken from Merker et al. [41]. It consists of three Lennard-Jones sites, representing each atom and a superimposed point quadrupole in the center of mass. The molecular model of toluene is taken from Huang et al. [3]. It consists of seven Lennard-Jones sites, five for the methine groups, one for the carbon atom and one for the methyl group, five point quadrupoles and one point dipole. The HCl model is also from Huang et al. [3]. It consists of one Lennard-Jones site and two partial charges, to account for polarity as well as hydrogen bonding [75, 76].

The total potential energy is given by

$$\begin{aligned} U = & \sum_{i=1}^{N-1}\sum_{j=i+1}^{N}\Biggl\{\sum_{a=1}^{n_i^{\mathrm{LJ}}}\sum_{b=1}^{n_j^{\mathrm{LJ}}}4\epsilon_{ijab}\left[\left(\frac{\sigma_{ijab}}{r_{ijab}}\right)^{12}-\left(\frac{\sigma_{ijab}}{r_{ijab}}\right)^{6}\right]+\sum_{c=1}^{n_i^{e}}\sum_{d=1}^{n_j^{e}}\frac{1}{4\pi\epsilon_0}\Biggl[\frac{q_{ic}q_{jd}}{r_{ijcd}} \\ & + \frac{q_{ic}\mu_{jd}+q_{jd}\mu_{ic}}{r_{ijcd}^{2}}\cdot f_1(\omega_i,\omega_j)+\frac{q_{ic}Q_{jd}+q_{jd}Q_{ic}}{r_{ijcd}^{3}}\cdot f_2(\omega_i,\omega_j)+\frac{\mu_{ic}\mu_{jd}}{r_{ijcd}^{3}}\cdot f_3(\omega_i,\omega_j) \\ & + \frac{\mu_{ic}Q_{jd}+\mu_{jd}Q_{ic}}{r_{ijcd}^{4}}\cdot f_4(\omega_i,\omega_j)+\frac{Q_{ic}Q_{jd}}{r_{ijcd}^{5}}\cdot f_5(\omega_i,\omega_j)\Biggr]\Biggr\}, \end{aligned} \tag{4}$$

where ϵ_{ijab} and σ_{ijab} are the Lennard-Jones energy and size parameters, r_{ijab} and r_{ijcd} are site-site distances, q_{ic}, q_{jd}, μ_{ic}, μ_{jd}, Q_{ic} and Q_{jd} are the magnitudes of the electrostatic interactions, i.e. the point charges, dipole and quadrupole moments, and $f_{\mathrm{k}}(\omega_i,\omega_j)$ are dimensionless angle-dependent expressions in terms of the orientation ω_i, ω_j of the point multipoles [77].

The unlike electrostatic interactions, e.g. between charges and quadrupoles, follow the laws of electrostatics, so that no combing rule is required. The modified Lorentz-Berthelot combining rules are used [78, 79] for the interaction between unlike Lennard-Jones sites

$$\sigma_{ij} = \frac{\sigma_{ii} + \sigma_{jj}}{2}, \tag{5}$$

$$\epsilon_{ij} = \xi\sqrt{\epsilon_{ii}\epsilon_{jj}}. \tag{6}$$

The binary interaction parameters ξ are usually fitted to experimental data of the vapor-liquid equilibrium [80]. For the binary subsystems, the interaction parameter ξ in the system toluene + HCl was taken from previous work [3] in which it was fitted to one experimental data point of the mixture and verified at another point. The interaction parameter in the system toluene + CO_2 was adjusted in the present work to fit the Henry's law constant of CO_2 in toluene at 353 K [81]. For HCl + CO_2, the binary interaction parameter was adjusted in the present work to fit the aceotropic pressure [18]. The binary interaction parameters are shown in Table 2.

[Table 2 about here.]

The MD simulations were performed with the MD code *ls*1 *mardyn* [40] in the canonical ensemble with N = 32,000 particles (except for the simulations of the Henry's law constant, see below). Simulation details are given in the Appendix. For the present MD simulations, systems were considered where the vapor and liquid phases coexist with each other in direct contact, employing periodic boundary conditions, so that there are two vapor-liquid interfaces which are oriented perpendicular to the y axis. The interfacial tension was computed from the deviation between the normal and the tangential diagonal components of the overall pressure tensor [61, 62]. For the mechanical route holds:

$$\gamma = \frac{1}{2S}\left(\Pi_{\mathrm{N}} - \Pi_{\mathrm{T}}\right) = \frac{1}{2}\int_{-\infty}^{\infty} \mathrm{d}y \left(p_{\mathrm{N}} - p_{\mathrm{T}}\right). \tag{7}$$

Thereby, the normal pressure p_{N} is given by the y component of the diagonal of the pressure tensor, and the tangential pressure p_{T} is determined by averaging over x and z components of the diagonal of the pressure tensor. The interfacial area S of each vapor-liquid interface is given by the cross section of the simulation volume normal to the y axis.

Thermodynamic properties in heterogeneous systems are very sensitive to the truncation of the intermolecular potential [50, 52, 82, 83]. This can either be treated by cutoff radii of the order of 10 times the segment diameter [50, 52, 84], which is numerically very expensive, or by an asymmetric long-range correction for inhomogeneous simulations [83–89].

For all of the present simulations, the cutoff radius was set to 17.5 Å and a center-of-mass cutoff scheme was employed. The Lennard-Jones interactions were corrected with a slab-based long-range correction [85]. Electrostatic long-range interactions were approximated by a resulting effective molecular dipole and corrected with a slab-based long-range correction [84]. The quadrupolar interactions do not need a long-range correction as they decay by r^{-10} [90].

The Henry's law constant $H_{i,\mathrm{Toluene}}$ of the solute i in the solvent toluene is given by

$$H_{i,\mathrm{Toluene}} = \rho_{\mathrm{Toluene}} k_{\mathrm{B}} T \exp\left(\frac{\mu_i^\infty}{k_{\mathrm{B}} T}\right), \tag{8}$$

where ρ_{Toluene} is the saturated liquid density of toluene and μ_i^∞ is the chemical potential of the solute at infinite dilution. The simulations of the Henry's law constant were performed with the $ms2$ simulation code [91, 92] with N = 1,000 particles. Simulation details are given in the Appendix.

2.3. Density gradient theory (DGT)

The interfacial tension γ of mixtures in VLE is calculated from equation (9) [93]

$$\gamma = \int_{\rho''_{\mathrm{ref}}}^{\rho'_{\mathrm{ref}}} \sqrt{2\Delta\Omega(\boldsymbol{\rho}) \sum_i \sum_j \kappa_{ij} \frac{\mathrm{d}\rho_i}{\mathrm{d}\rho_{\mathrm{ref}}} \frac{\mathrm{d}\rho_j}{\mathrm{d}\rho_{\mathrm{ref}}}} \mathrm{d}\rho_{\mathrm{ref}} \tag{9}$$

where $\boldsymbol{\rho}$ is the vector of component densities, ρ_i and ρ_j are the component densities of component i and j respectively, κ_{ij} is the so-called influence parameter of the component pair i and j, $\Delta\Omega(\boldsymbol{\rho}) = a_0(\boldsymbol{\rho}) - \sum_i \rho_i \mu_i^{\mathrm{bulk}} + p^{\mathrm{S}}$ is the grand potential per volume, with $a_0(\boldsymbol{\rho})$ being the homogeneous free energy at the local density vector, μ_i^{bulk} is the saturated bulk phase chemical potential of component i and p^{S} is the saturation pressure, ρ_{ref} is a suitably chosen reference density (which is that of the high boiling components density in our case). The summations run over all components and the integration is between the reference density at saturation in the vapor phase $\rho_{\mathrm{ref}}^{''}$ and the liquid phase $\rho_{\mathrm{ref}}^{'}$.

The component density profiles as a function of the spatial coordinate y are calculated from equation (10) [93]

$$\int_{y_0}^{y} \mathrm{d}y = \int_{\rho_{\mathrm{ref}}^{0}}^{\rho_{\mathrm{ref}}(y)} \sqrt{\Delta\Omega^{-1}(\boldsymbol{\rho}) \sum_i \sum_j \frac{1}{2} \kappa_{ij} \frac{\mathrm{d}\rho_i}{\mathrm{d}\rho_{\mathrm{ref}}} \frac{\mathrm{d}\rho_j}{\mathrm{d}\rho_{\mathrm{ref}}}} \mathrm{d}\rho_{\mathrm{ref}} \qquad (10)$$

where y_0 is an arbitrarily chosen starting point. For the remainder of this article we choose $\rho_{\mathrm{ref}}^{0} = 0.5\,(\rho_{\mathrm{ref}}^{'} + \rho_{\mathrm{ref}}^{''})$.

For the evaluation of equations (9) and (10), $\boldsymbol{\rho}$ has to be known as a function of ρ_{ref}. We assume, that the mixed influence parameter is calculated from the geometric mixing rule

$$\kappa_{ij} = \sqrt{\kappa_{ii}\kappa_{jj}}. \tag{11}$$

For that case, the relation between component densities is obtained from [93]

$$\sqrt{\kappa_{ii}}\Delta\mu_{\mathrm{ref}} = \sqrt{\kappa_{\mathrm{ref,ref}}}\Delta\mu_i, \tag{12}$$

where $\Delta\mu_i = \mu_i(\boldsymbol{\rho}) - \mu_i^{\mathrm{bulk}}$ is the difference between the chemical potential μ_i at $\boldsymbol{\rho}$ and the chemical potential at bulk conditions μ_i^{bulk}. The same definition holds for the chemical potential difference $\Delta\mu_{\mathrm{ref}}$ of the reference component. The influence parameter κ_{ii} of the pure component i is taken from the literature, where available, or fitted to one experimental data point of the pure component interfacial tension else.

2.4. PC-SAFT Equation of State

In this work we choose the Perturbed-Chain Statistical Associating Fluid Theory (PC-SAFT) [4, 5] as equation of state (EOS) for calculating the free energy of the homogeneous system, which is an extension of the SAFT EOS [94]. Like all perturbation theories, this EOS decomposes the free energy into different terms

$$A = A^{\mathrm{id}} + A^{\mathrm{hc}} + A^{\mathrm{disp}} + A^{\mathrm{assoc}}, \tag{13}$$

where A is the Helmholtz free energy and the subscripts id, hc, disp, and assoc stand for the contributions due to the ideal gas, the hard chain, the dispersion, and the association. The details of the EOS are described elsewhere [4, 5]. For non-associating compounds, the PC-SAFT EOS has three pure compound parameters, the segment number m, the segment diameter σ and the segment-segment interaction energy ϵ. For associating compounds, also the association volume κ^{AB} and the association energy ϵ^{AB} between two association sites A and B is used. Furthermore, in this case, the number of association sites of the types acidic, n_A, proton donor, n_P, and electron donor, n_E, has to be specified [95]. The pure component parameters for CO_2 and toluene were taken from the literature [4], whereas the pure component parameters for HCl were fitted to saturated densities, vapor pressures and enthalpies of vaporization from DIPPR correlations [96]. The influence parameters were taken from literature for CO_2 [97] and fitted to one experimental data point for toluene at 313.15 K [98] and for HCl at 220 K [96]. The parameters together with the specification of the way they were obtained are given in Table 3.

[Table 3 about here.]

Beside the pure compound parameters, PC-SAFT requires binary parameters k_{ij} for each binary mixture for the modified Berthelot-Lorentz combining rules

$$\sigma_{ij} = \frac{\sigma_{ii} + \sigma_{jj}}{2} \tag{14}$$

$$\epsilon_{ij} = (1 - k_{ij})\sqrt{\epsilon_{ii}\epsilon_{jj}}. \tag{15}$$

The parameters k_{ij} for the three binary subsystems were fitted to the same data as for the molecular force-field models, cf. Section 2.2, and are listed in Table 4.

[Table 4 about here.]

3. Results and Discussion

3.1. Pure component properties

The bulk properties of the three investigated pure fluids are determined by MD simulation of heterogeneous systems as well as the PC-SAFT EOS. The resulting saturated densities and the vapor pressure curves are shown in Figures 1 and 2, respectively. The simulated bulk properties are in very good agreement with the experimental data [96], which was already shown in previous publications, in which molecular simulations with the Grand Equilibrium method [3, 41, 99] were performed. Also the results from the PC-SAFT EOS [4] agree well with the experimental data. The new PC-SAFT model for HCl developed in the present work reproduces the saturated liquid density and the vapor pressure with a relative mean deviation of 1.2 % and 5.4 %, respectively.

[Figure 1 about here.]

[Figure 2 about here.]

The interfacial tension was not considered in the molecular model development so that the corresponding results are predictions. Figure 3 shows the interfacial tension as a function of the temperature for the three investigated fluids in comparison with DIPPR correlations to experimental data. The molecular models for toluene and CO_2 slightly overestimate the interfacial tension over the entire temperature range, while the HCl model shows a very good agreement with experimental data. The results from DGT + PC-SAFT are in very good agreement with the experimental data to which they were fitted (for CO_2 at 250 K [97], for Toluene at 313.15 K, for HCl at 220 K).

The numerical values of the MD simulation results for the VLE of the pure components are given in Table 5.

[Figure 3 about here.]

[Table 5 about here.]

3.2. Binary systems

3.2.1. Henry's law constant

Figure 4 shows the Henry's law constant for HCl and CO_2 in toluene as a function of the temperature. For HCl, these experimental data are only available at low temperatures [100–103]. The Henry's law constant from the present MD simulations is in very good agreement with the experimental data for both systems in the entire temperature range in which experimental data are available, which is narrow for HCl [81, 100–111]. For low temperatures the PC-SAFT results for the Henry's law constant of HCl in toluene are higher than the experimental values, which have not been used for the adjustment for the binary interaction parameter. Generally, the results from both methods agree well, both methods predict a maximum of the Henry's law constant at high temperatures, which remains to be confirmed by experiments.

The numerical values of the MD simulation results for the Henry's law constant are given in Table 6.

[Figure 4 about here.]

[Table 6 about here.]

3.2.2. Vapor-liquid equilibrium

VLE in the binary systems toluene + CO_2 and toluene + HCl were investigated at 333 and 353 K. Figures 5 and 6 show the binary phase diagrams. In the binary mixture toluene + CO_2, good agreement of the MD simulation results with the experimental data [9–17] is found over the entire concentration range, cf. Figure 5. There is an excellent agreement between MD simulation and PC-SAFT for low pressures, whereas, there are deviations at higher pressures. For the system toluene + HCl, cf. Figure 6, no experimental data are available for comparison. There is again a good agreement of both methods for the gas solubility as could be expected from the results shown in Figure 4. There are again some deviations in the pressure for higher concentrations of HCl in the liquid phase and also in the concentration of toluene in the gas phase. The sign of these deviations is not the same for the two systems studied here.

[Figure 5 about here.]

[Figure 6 about here.]

3.2.3. Interfacial tension

On the basis of well described phase equilibria, the interfacial properties can be predicted. Figure 7 shows the interfacial tension of toluene + CO_2 mixtures as a function of the mole fraction of CO_2 in the liquid phase. The interfacial tension of pure toluene is overpredicted by the molecular model at both temperatures. Experimental data are only available for pure toluene. The interfacial tension predicted by the molecular models decreases almost linearly with the mole fraction of CO_2 in the liquid phase, going to zero at the critical point. The results for the DGT + PC-SAFT are in good agreement with pure component data as they were fitted to such data. They also predict a linear decrease of the interfacial tension as a function of the mole fraction of CO_2 in the liquid phase, except in the vicinity of the critical point.

[Figure 7 about here.]

Figure 8 shows the interfacial tension of toluene + HCl mixtures as a function of the mole fraction of HCl in the liquid phase. The interfacial tension decreases nonlinearly with the mole fraction of HCl in the liquid phase. The MD simulations results are again higher than the simulations results from DGT + PC-SAFT, which can be attributed to the deviation for the pure component model for toluene. The nonlinear decrease of the interfacial tension is consistently predicted by both methods.

[Figure 8 about here.]

3.2.4. Density profiles and interfacial adsorption

The employed methods allow to resolve the interface on the length scale of nm. Figures 9 and 10 show density profiles of the binary systems toluene + CO_2 and toluene + HCl at 333 K and a low concentration of the light-boiling component in the liquid phase as a function of the coordinate normal to the interface as obtained with both methods. The component density of the high boiling component changes monotonously from the vapor to the liquid phase and so does the total density. The component density of the low boiling component exhibits a maximum at the interface. This maximum is predicted by MD simulations as well as DGT + PC-SAFT. The width of this density peak of CO_2, cf. Figure 9, at the interface is slightly narrower for the DGT + PC-SAFT, but the density maximum is slightly higher. This might be attributed to fluctuations at the interface in the MD simulation. For HCl, cf. Figure 10, the density maximum is smaller for DGT + PC-SAFT as compared to the MD simulation while the width is similar for both methods. Considering the fact that two completely independent methods were used for the predictions the results agree remarkably well.

[Figure 9 about here.]

[Figure 10 about here.]

Figures 11 and 12 show the results for the interfacial enrichment E_i, cf. equation (2), as a function of the mole fraction of the light boiling component in the liquid phase for the light boiling components i = CO_2, HCl in binary mixtures with toluene. In the VLE of the systems toluene + CO_2, the component density of CO_2 at the interface is up to three times larger than the component density in the bulk liquid phase, cf. Figure 11. The interfacial enrichment decreases with increasing mole fraction of CO_2 in the liquid phase and is higher at lower temperatures. The DGT + PC-SAFT results for the interfacial enrichment of CO_2 are slightly higher than the MD simulation results, except for a single value for each temperature, with the smallest mole fraction of CO_2 in the liquid phase.

In the VLE of the system toluene + HCl, an enrichment up to 2 is calculated from the MD simulation and up to 1.5 for DGT + PC-SAFT, cf.

Figure 12. The interfacial enrichment decreases with the mole fraction of HCl in the liquid phase and is more pronounced for lower temperatures. The results for DGT + PC-SAFT are lower for the interfacial enrichment of HCl than the results from the MD simulations.

The DGT + PC-SAFT results show in both mixtures an almost linear decrease of the interfacial enrichment with increasing mole fraction of the light boiling component in the liquid phase, whereas the MD simulation results show a non-linear decrease. For both systems, the numerical values of E_i converge to one at the critical point. At the critical point both phases are equal and no enrichment can occur.

[Figure 11 about here.]

[Figure 12 about here.]

Figure 13 shows the relative adsorption of CO_2 in VLE of binary mixtures with toluene at the interface as a function of the mole fraction of CO_2 in the liquid phase as obtained from the results of both methods using equation (3). Starting at low loadings the relative adsorption of CO_2 at the interface increases for an increasing mole fraction of CO_2. Close to the critical point the relative adsorption exhibits a maximum and decreases rapidly towards zero at the critical point. The relative adsorption decreases with increasing temperature. The results of the MD simulations are smaller compared to the DGT + PC-SAFT results, but the trends are consistently predicted by both methods.

Figure 14 shows the relative adsorption of HCl in VLE of binary mixtures with toluene at the interface as a function of the mole fraction of HCl in the liquid phase. The trends are similar to those observed for the system with CO_2, but the influence of temperature is smaller. The results of the MD simulations are higher than the those obtained with DGT + PC-SAFT, but again the trends predicted by both methods agree well.

The numerical values of the relative adsorption of CO_2 and HCl are similar, even though CO_2 shows a stronger interfacial enrichment E_i, thus emphasizing the importance to take both quantities into consideration.

[Figure 13 about here.]

[Figure 14 about here.]

The numerical values of the MD simulation results for the VLE of the binary systems are given in Tables 7 and 8. Results for the VLE in binary mixture CO_2 + HCl and for the relative adsorption based on the Gibbs adsorption equation instead of the density profiles as a check for consistency are given in the Supplementary information.

[Table 7 about here.]

[Table 8 about here.]

3.3. Ternary system

MD as well as DGT + PC-SAFT simulations of the VLE of the ternary system were carried out at 353 K and 4.9 MPa. Figure 15 shows the results, which are predictions by both methods, as no ternary interaction parameters were used. The results predicted by PC-SAFT show almost straight bubble and dew line. The results for the dew line match those from the MD simulations well, whereas for the bubble line some deviations occur which are partially due to the differences in the binary system toluene + HCl.

[Figure 15 about here.]

The corresponding interfacial tension of the ternary system as a function of the mole fraction of CO_2 in the liquid phase is shown in Figure 16. The interfacial tensions in the binary systems toluene + CO_2 and toluene + HCl are similar. In the ternary system the interfacial tension depends only weakly on the ratio of the two light-boiling components with a slight maximum, which is predicted by both methods. The interfacial tension predicted by the MD simulations is approximately 20 % higher than the corresponding values predicted by DGT + PC-SAFT. This overestimation can again be attributed to the pure component model for toluene.

[Figure 16 about here.]

In Figure 17, the density profiles of a ternary system toluene + CO_2 + HCl at 353 K with $x'_{\mathrm{CO_2}} = 0.12$ mol mol^{-1} and $x'_{\mathrm{HCl}} = 0.30$ mol mol^{-1} are shown as a function of the coordinate y normal to the interface. Both CO_2 and HCl show an enrichment at the interface. The results match well to those for the binary subsystems. No cross-interaction can be detected between the two enriching components.

[Figure 17 about here.]

This is confirmed by the interfacial enrichment of the light-boiling components CO_2 and HCl in VLE of the ternary mixture with toluene, which is shown in Figure 18 as a function of the mole fraction of CO_2 in the liquid phase. The results from the MD simulations for the interfacial enrichment of CO_2 are almost constant over the entire concentration range, whereas the

DGT + PC-SAFT results for the interfacial enrichment of CO_2 are increasing with increasing mole fraction of CO_2 in the liquid phase. The DGT + PC-SAFT and the MD simulations agree favorably for the interfacial enrichment of HCl, which changes only very slightly. The interfacial enrichment of the individual components is not strongly influenced by the presence of the other light boiling component. The numerical values for the enrichment predicted by the DGT + PC-SAFT are again higher for CO_2 and lower for HCl compared to the MD simulation results.

[Figure 18 about here.]

The relative adsorption of both light-boiling components in VLE of the ternary mixture with toluene is shown in Figure 19. The relative adsorption of CO_2 is increasing with increasing the liquid mole fraction of CO_2. Whereas increasing the mole fraction of HCl in the liquid phase increases the relative adsorption of HCl. The total relative adsorption is almost independent of the composition, which confirms that the two supercritical components do not influence each other at the vapor-liquid interface. Both methods agree favorably.

The numerical values of the MD simulation results for the VLE in the ternary system are given in Table 9.

[Figure 19 about here.]

[Table 9 about here.]

4. Conclusion

In the present work, interfacial and bulk properties of mixtures containing toluene, CO_2 and HCl were determined with MD simulations and DGT + PC-SAFT. The results from the present work for the bulk properties are in very good agreement with experimental data. The predictions obtained with the MD simulations for the interfacial tension is slightly too high for CO_2 and toluene, while for HCl very good agreement with experimental data is observed. The DGT + PC-SAFT results are in very good agreement with experimental data for the interfacial tension of the pure components. The interfacial tensions of binary and ternary mixtures, for which no experimental data are available, are predicted.

In the systems with toluene, CO_2 and HCl adsorb at the vapor-liquid interface. The local component density of the light boiling component (i.e. CO_2 or HCl, or both) reaches up to three times the value of the liquid phase. In the ternary system with toluene, both CO_2 and HCl adsorb at the vapor-liquid interface. The numerical values of the relative adsorption of CO_2 and

HCl in binary mixtures with toluene in VLE are similar, even though CO_2 shows a stronger interfacial enrichment. In the ternary system, the total relative adsorption is almost independent of the composition of the liquid phase. Interestingly, no significant interdependence between both enriching components is found.

The present study indicates that significant non-trivial interfacial effects occur in wide-boiling mixtures. In light of the strictly predictive character of the present results, attention should be paid to the fact that the results were confirmed by two independent theoretical methods. Enrichment effects at the interface influence heat and mass transfer. Mass transfer, e.g., is commonly described using the Fickian approach. Thereby the mass transfer is proportional to the density gradient of the individual components. This definition is incompatible with the density profiles from the present work. Therefore, a new definition for the diffusion at fluid interfaces is necessary.

Acknowledgement

The authors gratefully acknowledge financial support from BMBF within the SkaSim project (grant no. 01H13005A) and from Deutsche Forschungsgemeinschaft (DFG) within the Collaborative Research Center (SFB) 926. The present work was conducted under the auspices of the Boltzmann-Zuse Society of Computational Molecular Engineering (BZS) and the simulations were carried out on the Regional University Computing Center Kaiserslautern (RHRK) under the grant TUKL-MSWS as well as on JUQUEEN at Jülich Supercomputing Center under the grant HKL09 within the PARSIVAL scientific computing project.

Appendix A. Molecular simulation details

Appendix A.1. Heterogeneous simulations of vapor-liquid equilibria

The equations of motion were solved by a leapfrog integrator [112] with a time step of $\Delta t = 1$ fs. The elongation of the simulation volume normal to the interface was at least 30 nm and the thickness of the liquid film in the center of the simulation volume was 15 nm, which limits the influence of finite size effects on the simulation outcome [113]. The elongation in the other spatial directions was at least 6 nm. The equilibration ran for at least 500,000 time steps, to ensure fully equilibrated systems. The production ran for 2,500,000 time steps to reduce statistical uncertainties. The statistical errors were estimated to be three times the standard deviation of five block averages, each over 500,000 time steps. The saturated densities, compositions and vapor pressures were calculated as an average over the respective phases, excluding the regions close to the interface.

Appendix A.2. Henry's law constant simulations

Widom's test particle insertion was used to calculate the chemical potential [114]. The fluid was equilibrated over 200,000 time steps in the canonical (NVT) ensemble. The production run in the isobaric-isothermal (NpT) ensemble went over 200,000 time steps with a piston coupling constant of 10^9 kg/m^4. Up to 5000 test molecules were inserted in every production time step. The Lennard-Jones interactions were corrected with the angle-averaging scheme proposed by Lustig [115]. Electrostatic long-range interactions were calculated using the reaction field method [116].

[1] B. Eckl, J. Vrabec, and H. Hasse. *Fluid Phase Equilib.*, 274:16–26, 2008.

[2] Y.-L. Huang, T. Merker, M. Heilig, H. Hasse, and J. Vrabec. *Ind. Eng. Chem. Res.*, 51:7428–7440, 2012.

[3] Y.-L. Huang, M. Heilig, H. Hasse, and J. Vrabec. *AIChE J.*, 57(4):1043–1060, 2011.

[4] J. Gross and G. Sadowski. *Ind. Eng. Chem. Res.*, 40(4):1244, 2001.

[5] J. Gross and G. Sadowski. *Ind. Eng. Chem. Res.*, 41(22):5510–5515, 2002.

[6] H. Kahl and S. Enders. *Phys. Chem. Chem. Phys.*, 4:931–936, 2002.

[7] S. Enders and H. Kahl. *Fluid Phase Equilib.*, 263(2):160–167, 2008.

[8] P. M. W. Cornelisse, C. J. Peters and J. de Swaan Arons. *Fluid Phase Equilib.*, 117:312–319, 1996.

[9] L.-B. Chen and X.-G. Fang. *J. Nat. Gas Chem.*, 3:255–266, 1994.

[10] Z. Yang, M. Li, B. Peng, and Z. Dong. *J. Chem. Eng. Data*, 57(4):1305–1311, 2012.

[11] K. Tochigi, K. Hasegawa, N. Asano, and K. Kojima. *J. Chem. Eng. Data*, 43(6):954–956, 1998.

[12] S.-D. Park, C.-H. Kim, and C.-S. Choi. *Hwahak Konghak*, 28(4):438–443, 1990.

[13] P. Naidoo, D. Ramjugernath, and J. D. Raal. *Fluid Phase Equilib.*, 269(1-2):104–112, 2008.

[14] W. O. Morris and M. D. Donohue. *J. Chem. Eng. Data*, 30(3):259–263, 1985.

[15] A. L. Muhlbauer and J. D. Raal. *Fluid Phase Equilib.*, 64:213–236, 1991.

[16] C.-H. Kim, P. Vimalchand, and M. D. Donohue. *Fluid Phase Equilib.*, 31(3):299–311, 1986.

[17] D. Walther, B. Platzer, and G. Maurer. *J. Chem. Thermodyn.*, 24(4):387–399, 1992.

[18] G. Ansdell. *Proc. Roy. Soc. London*, 34:113–119, 1882.

[19] C. Dorsman. *Isothermen van Mengsels van Zoutzuur en Koolzuur.* PhD thesis, Univ. van Amsterdam, 1908.

[20] B. U. Felderhof. *Physica*, 48(4):541–560, 1970.

[21] J. Vrabec, G. K. Kedia, G. Fuchs, and H. Hasse. *Mol. Phys.*, 104(9):1509–1527, 2006.

[22] S. Eckelsbach and J. Vrabec. *Phys. Chem. Chem. Phys.*, 17(40):27195–27203, 2015.

[23] T. Wadewitz and J. Winkelmann. *Ber. Bunsen-Ges. Phys. Chem.*, 100(11):1825–1832, 1996.

[24] C. I. Poser and I. C. Sanchez. *Macromol.*, 14(2):361–370, 1981.

[25] O. G. Niño-Amézquita, S. Enders, P. T. Jaeger, and R. Eggers. *Ind. Eng. Chem. Res.*, 49(2):592–601, 2010.

[26] E. Schäfer, G. Sadowski, and S. Enders. *Fluid Phase Equilib.*, 362:151–162, 2014.

[27] J.-C. Neyt, A. Wender, V. Lachet, and P. Malfreyt. *J. Phys. Chem. C*, 116(19):10563–10572, 2012.

[28] C. Miqueu, J. M. Míguez, M. M. Piñeiro, T. Lafitte, and B. Mendiboure. *J. Phys. Chem. B*, 115(31):9618–9625, 2011.

[29] F. Biscay, A. Ghoufi, V. Lachet, and P. Malfreyt. *J. Phys. Chem. B*, 113(43):14277–14290, 2009.

[30] E. A. Müller and A. Mejía. *Fluid Phase Equilib.*, 282(2):68–81, 2009.

[31] H. Lin, Y.-Y. Duan, and Q. Min. *Fluid Phase Equilib.*, 254(1-2):75–90, 2007.

[32] M. Sahimi and B. N. Taylor. *J. Chem. Phys.*, 95(9):6749–6761, 1991.

[33] O. G. Niño-Amézquita, D. van Putten, and S. Enders. *Fluid Phase Equilib.*, 332:40–47, 2012.

[34] H. Cárdenas and A. Mejía. *Mol. Phys.*, in press, 2016. DOI: 10.1080/00268976.2016.1170221.

[35] X.-S. Li, J.-M. Liu, and D. Fu. *Ind. Eng. Chem. Res.*, 47(22):8911–8917, 2008.

[36] T. Lafitte, B. Mendiboure, M. M. Piñeiro, D. Bessières, and C. Miqueu. *J. Phys. Chem. B*, 114(34):11110–11116, 2010.

[37] O. Lobanova, A. Mejía, G. Jackson, and E. A. Müller. *J. Chem. Thermodyn.*, 93:320–336, 2016.

[38] W. Shi, N. S. Siefert, and B. D. Morreale. *J. Phys. Chem. C*, 119(33):19253–19265, 2015.

[39] C. Bühl, A. Denzer, and S. Enders. *Fluid Phase Equilib.*, 416:94–103, 2016.

[40] C. Niethammer, S. Becker, M. Bernreuther, M. Buchholz, W. Eckhardt, A. Heinecke, S. Werth, H.-J. Bungartz, C. W. Glass, H. Hasse, J. Vrabec, and M. Horsch. *J. Chem. Theory Comput.*, 10(10):4455–4464, 2014.

[41] T. Merker, C. Engin, J. Vrabec, and H. Hasse. *J. Chem. Phys.*, 132:234512, 2010.

[42] G. Guevara-Carrión, J. Vrabec, and H. Hasse. *Fluid Phase Equilib.*, 316:46–54, 2012.

[43] J. Vrabec, J. Stoll, and H. Hasse. *J. Phys. Chem. B*, 105(48):12126–12133, 2001.

[44] J. Stoll, J. Vrabec, and H. Hasse. *J. Chem. Phys.*, 119(21):11396–11407, 2003.

[45] S. Eckelsbach, S. Miroshnichenko, G. Rutkai, and J. Vrabec. In W. E. Nagel, D. B. Kröner, and M. M. Resch, editors, *High Performance Computing in Science and Engineering '13*, pages 635–646. Springer, Berlin/Heidelberg, 2013.

[46] J.-C. Neyt, A. Wender, V. Lachet, and P. Malfreyt. *J. Phys. Chem. B*, 115(30):9421–9430, 2011.

[47] S. Werth, K. Stöbener, P. Klein, K.-H. Küfer, M. Horsch, and H. Hasse. *Chem. Eng. Sci.*, 121:110–117, 2015.

[48] S. Werth, M. Horsch, and H. Hasse. *J. Chem. Phys.*, 144:054702, 2016.

[49] C. Caleman, P. J. van Maaren, M. Hong, J. S. Hub, L. T. Costa, and D. van der Spoel. *J. Chem. Theory Comput.*, 8(1):61–74, 2012.

[50] R. A. Zubillaga, A. Labastida, B. Cruz, J. C. Martínez, E. Sánchez, and J. Alejandre. *J. Chem. Theory Comput.*, 9(3):1611–1615, 2013.

[51] C. Avendaño, T. Lafitte, A. Galindo, C. S. Adjiman, G. Jackson, and E. A. Müller. *J. Phys. Chem. B*, 115(38):11154–11169, 2011.

[52] C. Avendaño, T. Lafitte, C. S. Adjiman, A. Galindo, E. A. Müller, and G. Jackson. *J. Phys. Chem. B*, 117(9):2717–2733, 2013.

[53] C. Herdes, T. S. Totton, and E. A. Müller. *Fluid Phase Equilib.*, 406:91–100, 2015.

[54] N. Ferrando, V. Lachet, J. Pérez-Pellitero, A. D. Mackie, and P. Malfreyt. *J. Phys. Chem. B*, 115(36):10654–10664, 2011.

[55] S. K. Singh, A. Sinha, G. Deo, and J. K. Singh. *J. Phys. Chem. C*, 113(17):7170–7180, 2009.

[56] N. M. Fischer, P. J. van Maaren, J. C. Ditz, A. Yildirim, and D. van der Spoel. *J. Chem. Theory Comput.*, 11(7):2938–2944, 2015.

[57] K. Stöbener, P. Klein, S. Reiser, M. Horsch, K.-H. Küfer, and H. Hasse. *Fluid Phase Equilib.*, 373:100–108, 2014.

[58] K. Stöbener, P. Klein, M. Horsch, K.-H. Küfer, and H. Hasse. *Fluid Phase Equilib.*, 411:33–42, 2015.

[59] J. D. van der Waals. *Over de Continuiteit van den Gas- en Vloeistoftoestand*. PhD thesis, Universiteit Leiden, 1873.

[60] J. W. Cahn and J. E. Hilliard. *J. Chem. Phys.*, 28(2):258–267, 1958.

[61] J. P. R. B. Walton, D. J. Tildesley, J. S. Rowlinson, and J. R. Henderson. *Mol. Phys.*, 48(6):1357–1368, 1983.

[62] J. G. Kirkwood and F. P. Buff. *J. Chem. Phys.*, 17(3):338–343, 1949.

[63] E. Salomons and M. Mareschal. *J. Phys.: Cond. Mat.*, 3(20):3645–3661, 1991.

[64] G. J. Gloor, G. Jackson, F. J. Blas, and E. de Miguel. *J. Chem. Phys.*, 123:134703, 2005.

[65] A. Ghoufi and P. Malfreyt. *J. Chem. Phys.*, 136:024104, 2012.

[66] K. Binder. *Z. Phys. B*, 43:119–140, 1981.

[67] K. Binder. *Phys. Rev. A*, 25(3):1699–1709, 1982.

[68] M. Schrader, P. Virnau, D. Winter, T. Zykova-Timan, and K. Binder. *Eur. Phys. J. Spec. Top.*, 117(1):103–127, 2009.

[69] S. K. Das and K. Binder. *Phys. Rev. Lett.*, 107:235702, 2011.

[70] A. Tröster, M. Oettel, B. Block, P. Virnau, and K. Binder. *J. Chem. Phys.*, 136:064709, 2012.

[71] G. V. Lau, I. J. Ford, P. A. Hunt, E. A. Müller, and G. Jackson. *J. Chem. Phys.*, 142:114701, 2015.

[72] J. G. Sampayo, A. Malijevský, E. A. Müller, E. de Miguel, and G. Jackson. *J. Chem. Phys.*, 132:141101, 2010.

[73] A. Malijevský and G. Jackson. *J. Phys.: Cond. Mat.*, 24:464121, 2012.

[74] J. W. Gibbs. *The Scientific Papers of J. W. Gibbs.* Dover Publications, 1961.

[75] S. Reiser, N. McCann, M. Horsch, and H. Hasse. *J. Supercrit. Fluids*, 68:94–103, 2012.

[76] K. Langenbach, C. Engin, S. Reiser, M. Horsch, and H. Hasse. *AIChE J.*, 61(9):2926–2932, 2015.

[77] C. G. Gray and K. E. Gubbins. *Theory of Molecular Fluids, Vol. 1: Fundamentals*. Clarendon Press, Oxford, 1984.

[78] H. A. Lorentz. *Ann. Phys.*, 248:127–136, 1881.

[79] D. Berthelot. *Compt. Rend. Ac. Sc.*, 126:1703–1706, 1857–1858, 1898.

[80] T. Schnabel, J. Vrabec, and H. Hasse. *J. Mol. Liq.*, 135:170–178, 2007.

[81] S. D. Fink and H. C. Hershey. *Ind. Eng. Chem. Res.*, 29(2):295–306, 1990.

[82] S. Werth, M. Horsch, J. Vrabec, and H. Hasse. *J. Chem. Phys.*, 142:107101, 2015.

[83] C. L. Wennberg, T. Murtola, S. Páll, M. J. Abraham, B. Hess, and E. Lindahl. *J. Chem. Theory Comput.*, 11(12):5737–5746, 2015.

[84] S. Werth, M. Horsch, and H. Hasse. *Mol. Phys.*, 113(23):3750–3756, 2015.

[85] S. Werth, G. Rutkai, J. Vrabec, M. Horsch, and H. Hasse. *Mol. Phys.*, 112(17):2227–2234, 2014.

[86] R. E. Isele-Holder, W. Mitchell, and A. E. Ismail. *J. Chem. Phys.*, 137:174107, 2012.

[87] P. J. in't Veld, A. E. Ismail, and G. S. Grest. *J. Chem. Phys.*, 127:144711, 2007.

[88] D. Tameling, P. Springer, P. Bientinesi, and A. E. Ismail. *J. Chem. Phys.*, 140:024105, 2014.

[89] F. Goujon, A. Ghoufi, P. Malfreyt, and D. J. Tildesley. *J. Chem. Theory Comput.*, 11(10):4573–4585, 2015.

[90] J. M. Prausnitz, R. N. Lichtenthaler, and E. G. de Azevedo. *Molecular Thermodynamics of Fluid-Phase Equilibria.* Pearson Education, New Jersey, 1998.

[91] C. W. Glass, S. Reiser, G. Rutkai, S. Deublein, A. Köster, G. Guevara-Carrión, A. Wafai, M. Horsch, M. Bernreuther, T. Windmann, H. Hasse, and J. Vrabec. *Comp. Phys. Comm.*, 185(12):3302–3306, 2014.

[92] Y.-L. Huang, S. Miroshnichenko, H. Hasse, and J. Vrabec. *Int. J. Thermophys.*, 30(6):1791–1810, 2009.

[93] C. Miqueu, B. Mendiboure, A. Garciaa, and J. Lachaise. *Ind. Eng. Chem. Res.*, 44(9):3321–3329, 2005.

[94] W. G. Chapman, K. E. Gubbins, G. Jackson, and M. Radosz. *Fluid Phase Equilib.*, 52:31–38, 1989.

[95] K. Langenbach and S. Enders. *Mol. Phys.*, 110:1249–1260, 2012.

[96] R. L. Rowley, W. V. Wilding, J. L. Oscarson, Y. Yang, N. A. Zundel, T. E. Daubert, and R. P. Danner. *DIPPR Information and Data Evaluation Manager for the Design Institute for Physical Properties.* AIChE, 2013. Version 7.0.0.

[97] S. Enders, H. Kahl, and J. Winkelmann. *Fluid Phase Equilib.*, 228–229:511–522, 2005.

[98] A. P. Fröba and A. Leipertz. *Int. J. Thermophys.*, 24(4):895–921, 2003.

[99] J. Vrabec and H. Hasse. *Mol. Phys.*, 100(21):3375–3383, 2002.

[100] W. Ahmed, W. Gerrard, and V. K. Maladkar. *J. Appl. Chem.*, 20(4):109–116, 1970.

[101] R. P. Bell. *J. Chem. Soc. London*, pages 1371–1382, 1931.

[102] S. J. O'Brian and E. G. Bobalek. *J. Am. Chem. Soc.*, 62(11):3227–3230, 1940.

[103] H. C. Brown and J. D. Brady. *J. Am. Chem. Soc.*, 74(14):3570–3582, 1952.

[104] M. J. Horvath, H. M. Sebastian, and K.-C. Chao. *Ind. Eng. Chem. Fundam.*, 20(4):394–396, 1981.

[105] L. R. Field, E. Wilhelm, and R. Battino. *J. Chem. Thermodyn.*, 6(3):237–243, 1974.

[106] U. Waeterling, D. Zheng, and H. Knapp. *Chem. Eng. Process*, 29(3):155–164, 1991.

[107] H. M. Sebastian, J. J. Simnick, H.-M. Lin, and K.-C. Chao. *J. Chem. Eng. Data*, 25(3):246–248, 1980.

[108] H.-J. Ng and D. B. Robinson. *J. Chem. Eng. Data*, 23(4):325–327, 1978.

[109] L. Zhang, S. Han, and H. Knapp. *Chin. J. Chem. Eng.*, 4(2):168–173, 1996.

[110] L. Piskovsky and J. Lakomy. *J. Chem. Prum.*, 15(12):745–746, 1965.

[111] E. R. Shenderei, Y. D. Zelvenskii, and F. D. Ivanovskii. *Khim. Prom.*, 5:370–374, 1960.

[112] D. Fincham. *Mol. Sim.*, 8(3-5):165–178, 1992.

[113] S. Werth, S. V. Lishchuk, M. Horsch, and H. Hasse. *Physica A*, 392(10):2359–2367, 2013.

[114] B. Widom. *J. Chem. Phys.*, 39(11):2808–2812, 1963.

[115] R Lustig. *Mol. Phys.*, 65(1):175–179, 1988.

[116] J. A. Barker and R. O. Watts. *Mol. Phys.*, 26(3):789–792, 1973.

[117] R. Span and W. Wagner. *J. Phys. Chem. Ref. Data*, 25(6):1509–1596, 1996.

[118] E. W. Lemmon and R. Span. *J. Chem. Eng. Data*, 51:785–850, 2006.

[119] G. Rutkai, M. Thol, R. Lustig, R. Span, and J. Vrabec. *J. Chem. Phys.*, 139:041102, 2013.

[120] M. A. Kalbassi and M. W. Biddulph. *J. Chem. Eng. Data*, 33(4):473–476, 1988.

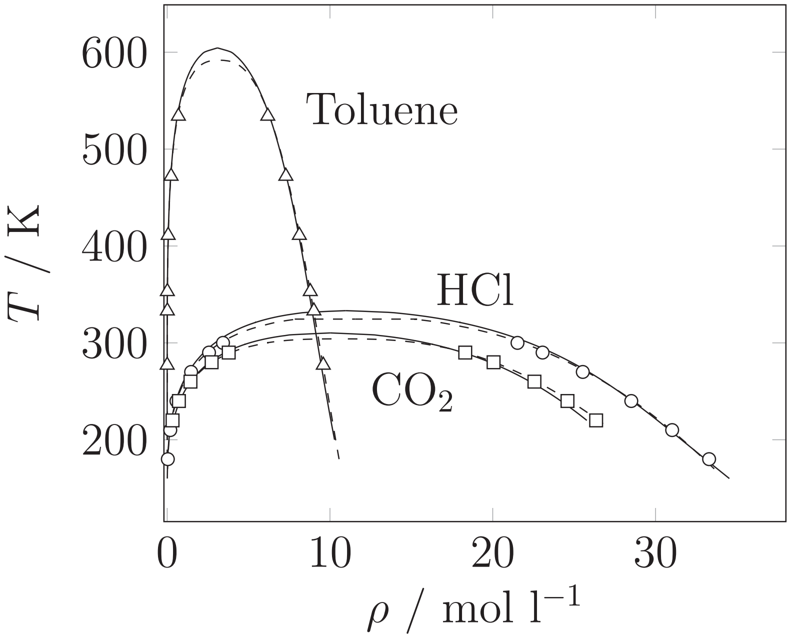

Figure 1: Saturated vapor and liquid densities of toluene (△), CO$_2$ (□) and HCl (○). Symbols are the present MD simulation results, solid lines are PC-SAFT results and dashed lines are results from correlations to experimental data (for CO$_2$ [117], toluene [118] and HCl [119]). The simulation uncertainties are smaller than the symbol size in all cases.

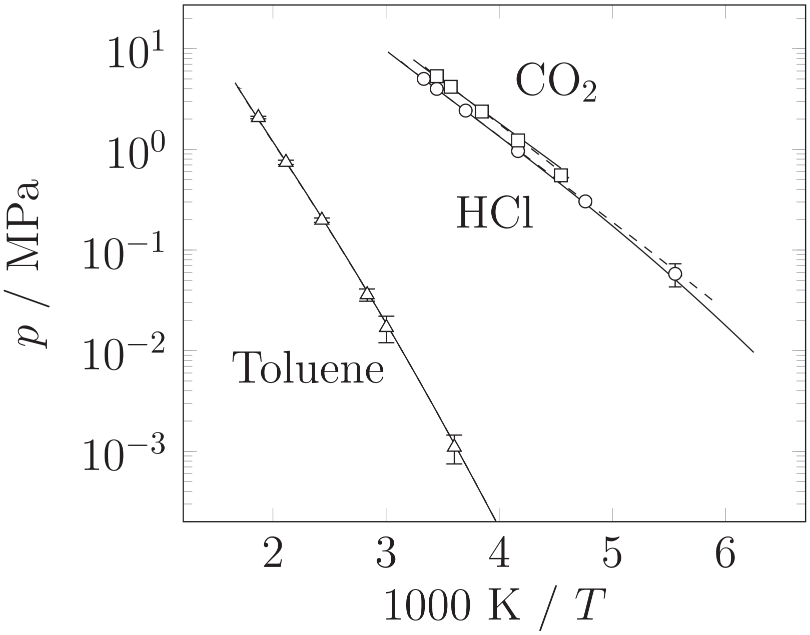

Figure 2: Vapor pressure curves of toluene (△), CO$_2$ (□) and HCl (○). Symbols are the present MD simulation results, the solid lines are PC-SAFT results and dashed lines are results from correlations to experimental data (for CO$_2$ [117], toluene [118] and HCl [119]).

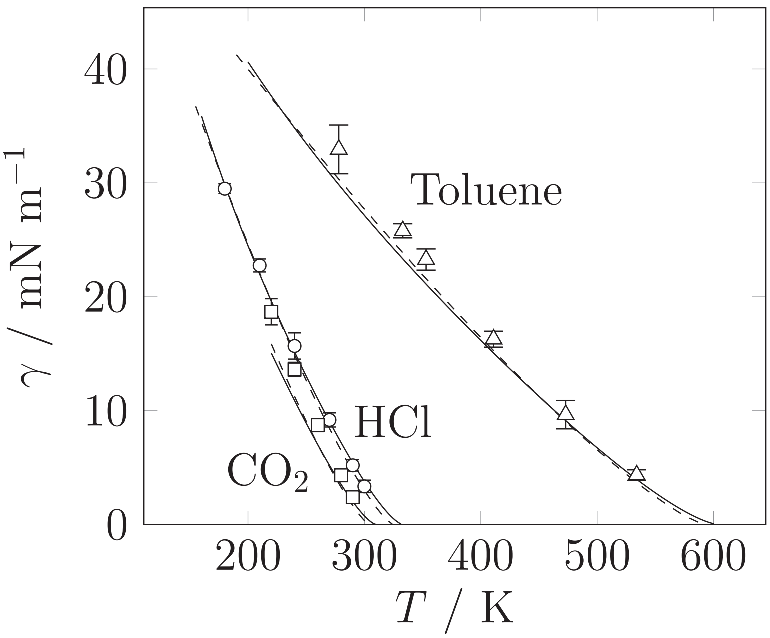

Figure 3: Interfacial tension of toluene (△), CO_2 (□) and HCl (○) as a function of the temperature. Symbols are the present MD simulation results, solid lines are DGT + PC-SAFT results and dashed lines are DIPPR correlations to experimental data [96].

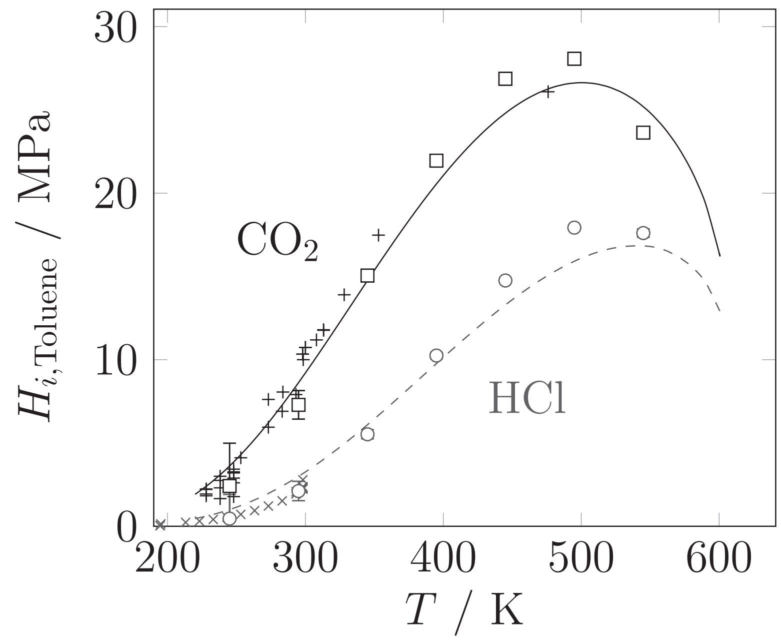

Figure 4: Henry's law constant of CO_2 (□, —–) and HCl (○, - - -) in toluene. Open symbols are the present MD simulation results, lines are PC-SAFT results, pluses are experimental data for CO_2 [81, 104–111], and crosses are experimental data for HCl [100–103].

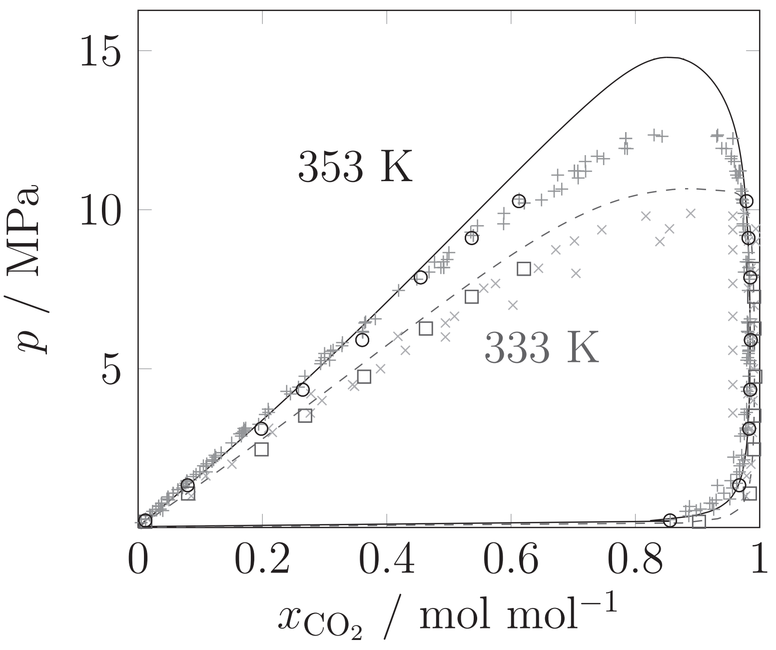

Figure 5: Vapor-liquid equilibrium of binary mixtures of toluene and CO_2 at 333 K (□, - - -) and 353 K (○, ——). Symbols are the present MD simulation results, lines are PC-SAFT results, crosses are experimental data at 333 K [9–13] and pluses are experimental data at 353 K [12–17].

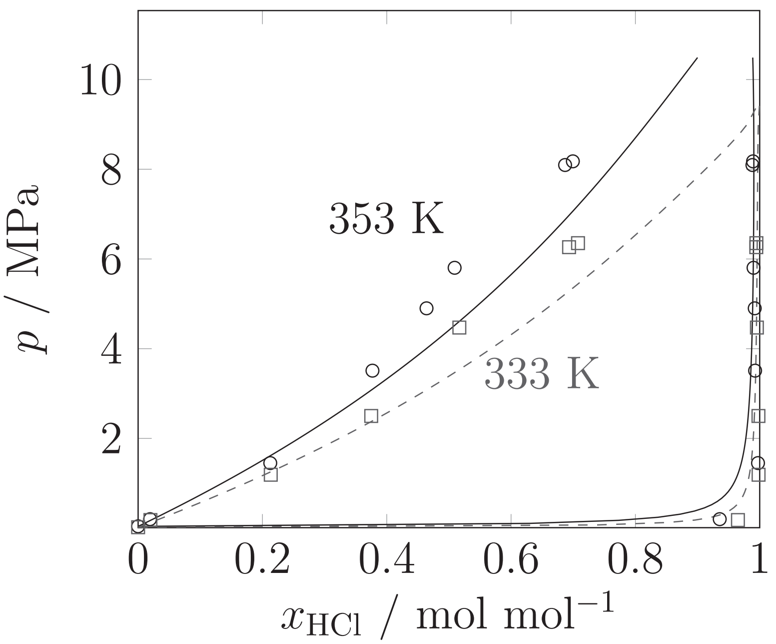

Figure 6: Vapor-liquid equilibrium of binary mixtures of toluene and HCl at 333 K (□, - - -) and 353 K (○, —). Symbols are the present MD simulation results and lines are PC-SAFT results. No experimental data are available.

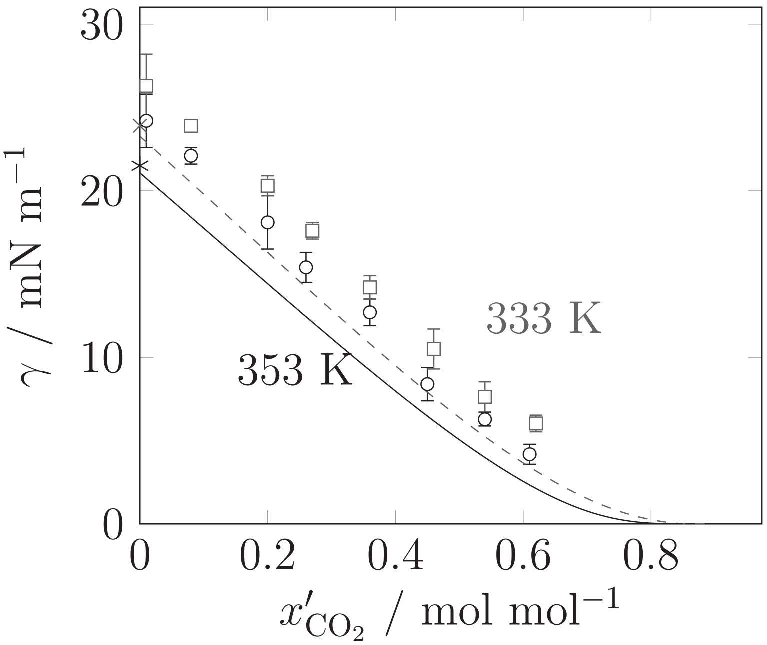

Figure 7: Interfacial tension of binary mixtures of toluene and CO_2 for 333 K (□, - - -) and 353 K (○, —–) as a function of the mole fraction of CO_2 of the liquid phase. Symbols are the present MD simulation results, lines are DGT + PC-SAFT results and crosses are experimental data for pure toluene [120].

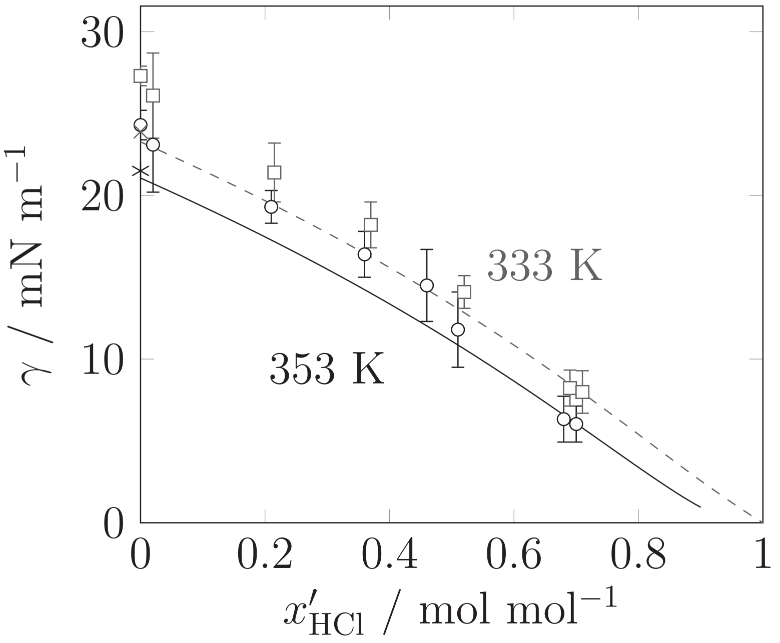

Figure 8: Interfacial tension of binary mixtures of toluene and HCl for 333 K (□, - - -) and 353 K (○, —) as a function of the mole fraction of HCl in the liquid phase. Symbols are the present MD simulation results, lines are DGT + PC-SAFT results and crosses are experimental data for pure toluene [120].

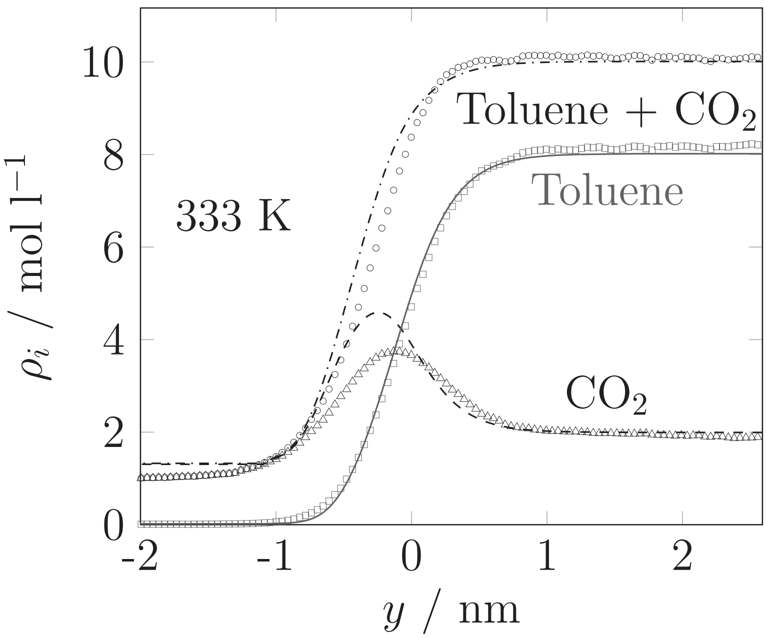

Figure 9: Density profiles of a binary mixture of toluene (□, ——) and CO$_2$ (△, - - -) as a function of the coordinate normal to the interface at T = 333 K and $x'_{\mathrm{CO_2}} \approx 0.2$ mol mol^{-1}. Symbols are the present MD simulations results and lines are DGT + PC-SAFT results.

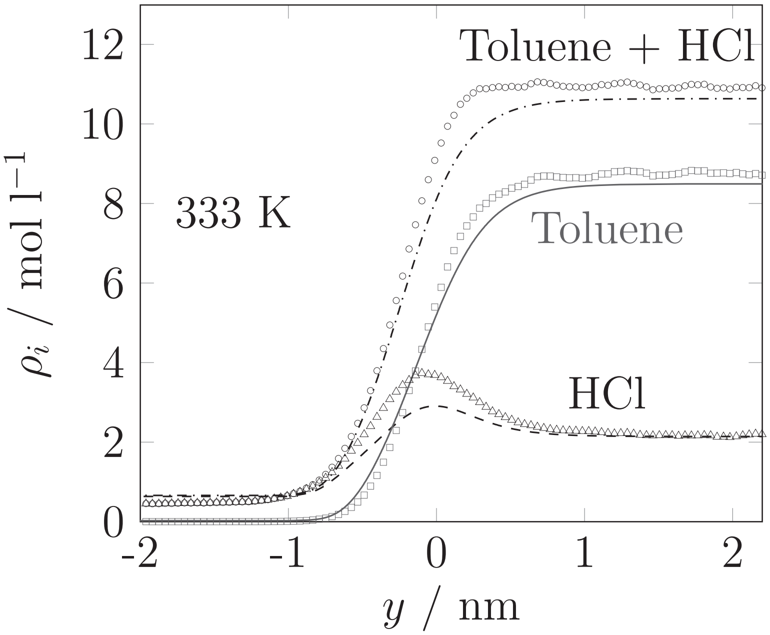

Figure 10: Density profiles of a binary mixture of toluene (□, —–) and HCl (△, - - -) as a function of the coordinate normal to the interface at $T = 333$ K and $x'_{\mathrm{HCl}} \approx 0.2$ mol mol^{-1}. Symbols are the present MD simulations results and lines are DGT + PC-SAFT results.

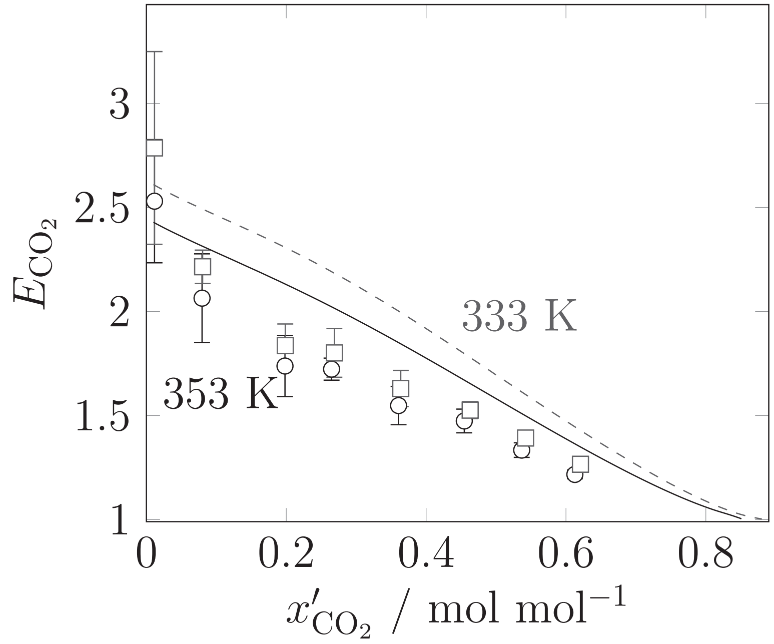

Figure 11: Interfacial enrichment of CO_2 as a function of the mole fraction of CO_2 in the liquid phase in binary mixtures with toluene in VLE for 333 K (□, - - -) and 353 K (○, —). Symbols are the present MD simulations results and lines are DGT + PC-SAFT results.

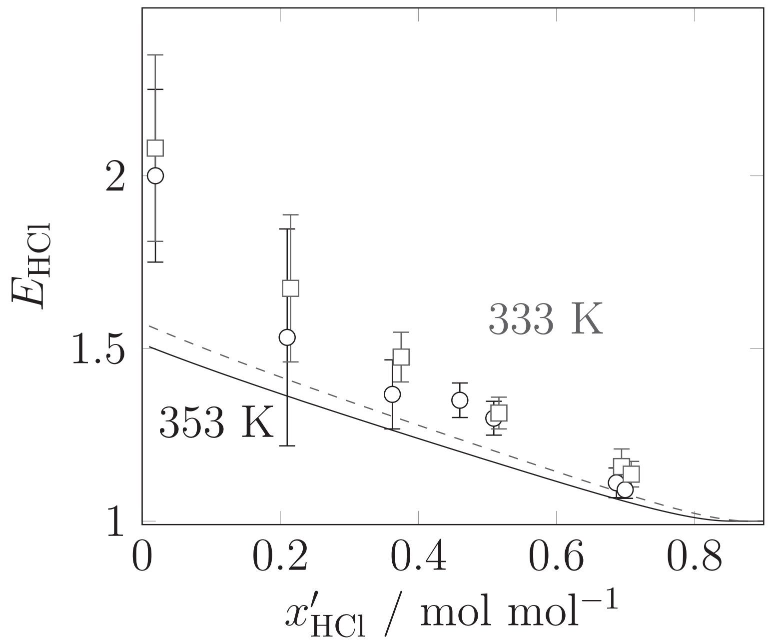

Figure 12: Interfacial enrichment of HCl as a function of the mole fraction of HCl in the liquid phase in binary mixtures with toluene in VLE for 333 K (□, - - -) and 353 K (○, —). Symbols are the present MD simulations results and lines are DGT + PC-SAFT results.

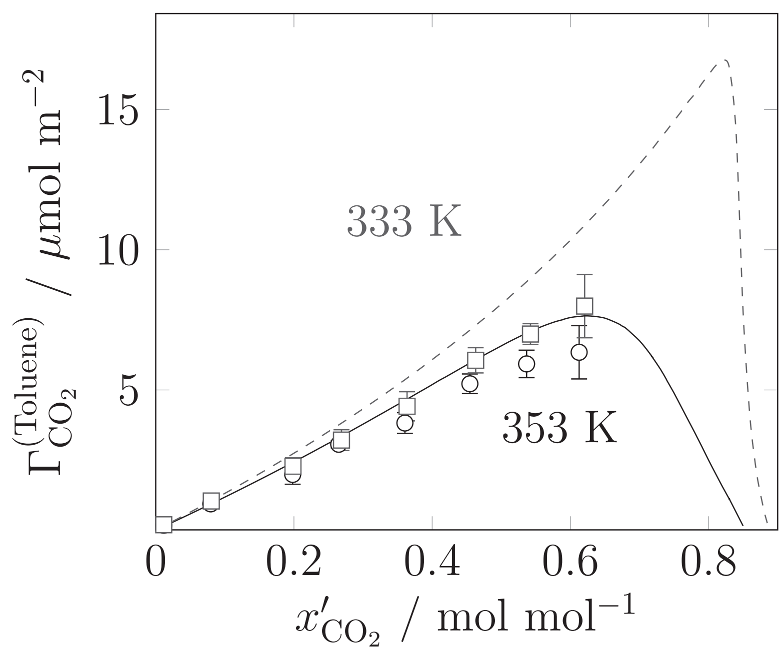

Figure 13: Relative adsorption of CO_2 at the interface defined such that $\Gamma_{\text{Toluene}} = 0$, as a function of the mole fraction of CO_2 in the liquid phase in binary mixtures with toluene in VLE for 333 K (□, - - -) and 353 K (○, ——). The Symbols are MD simulation results and the lines are DGT + PC-SAFT results.

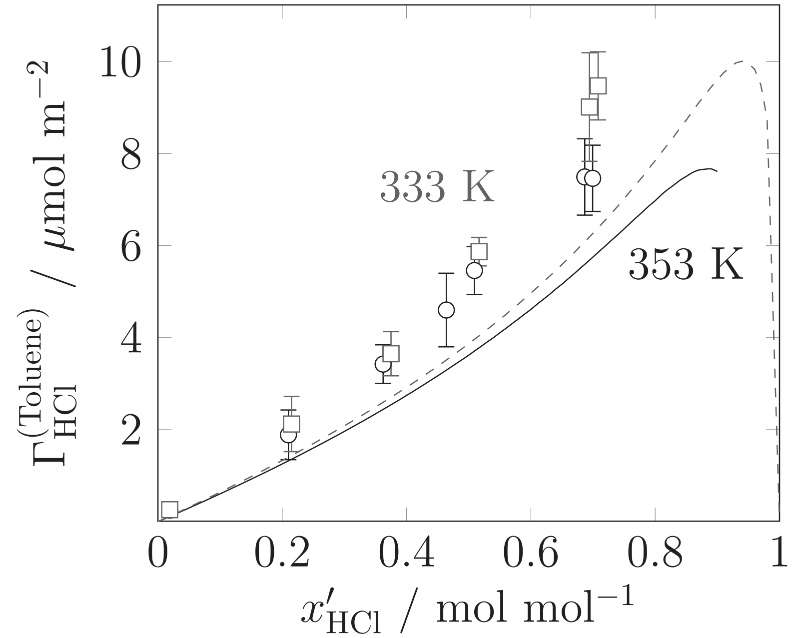

Figure 14: Relative adsorption of HCl at the interface defined such that $\Gamma_{\mathrm{Toluene}} = 0$, as a function of the mole fraction of HCl in the liquid phase in binary mixtures with toluene in VLE for 333 K (□, - - -) and 353 K (○, —–). The Symbols are MD simulation results and the lines are DGT + PC-SAFT results.

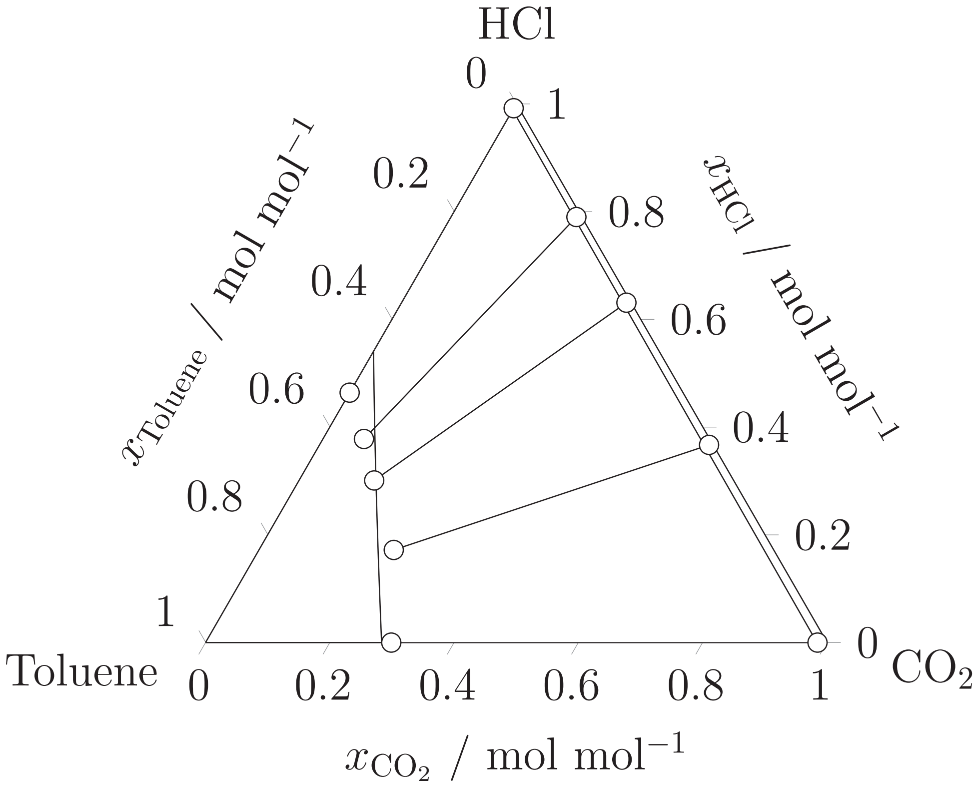

Figure 15: Vapor-liquid equilibrium compositions of the coexisting phases in the system toluene + CO_2 + HCl at T = 353 K and p = 4.9 MPa. Symbols are the present MD simulations results and lines are PC-SAFT results.

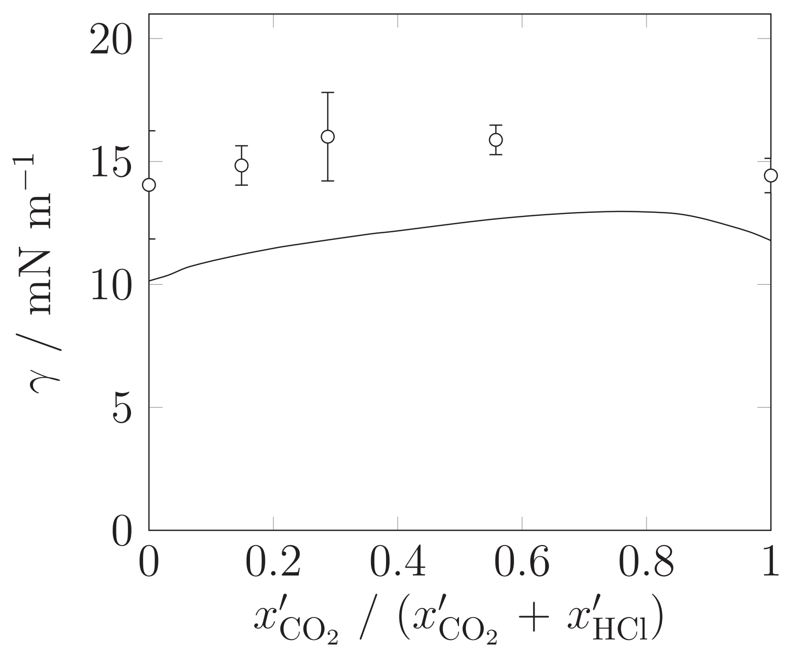

Figure 16: Interfacial tension of ternary mixtures toluene + CO_2 + HCl at $T = 353$ K and $p = 4.9$ MPa. Symbols are the present MD simulations results and the line is the DGT + PC-SAFT result.

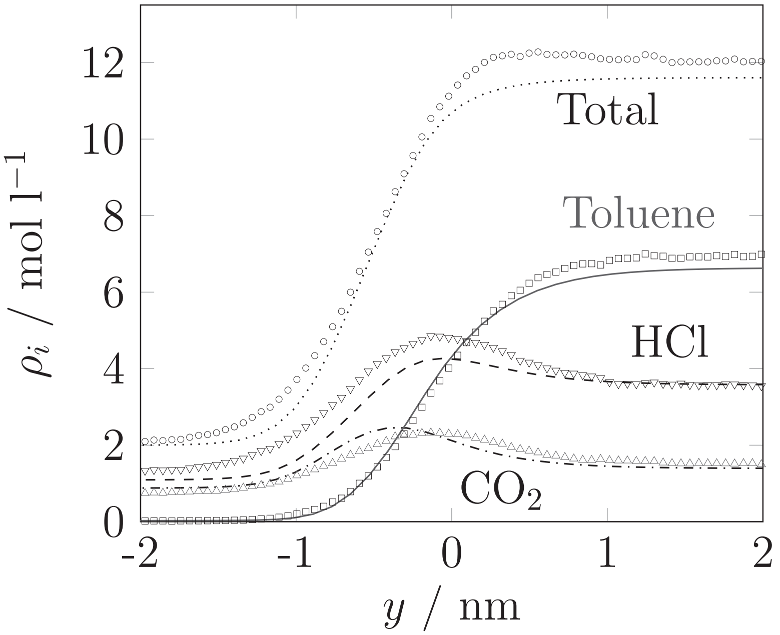

Figure 17: Density profiles of a ternary mixture of toluene (□), CO$_2$ (△) and HCl (▽) as a function of the coordinate normal to the interface at T = 353 K, p = 4.9 MPa and x'_{CO_2} = 0.12 mol mol^{-1}. Symbols are the present MD simulations results and lines are DGT + PC-SAFT results.

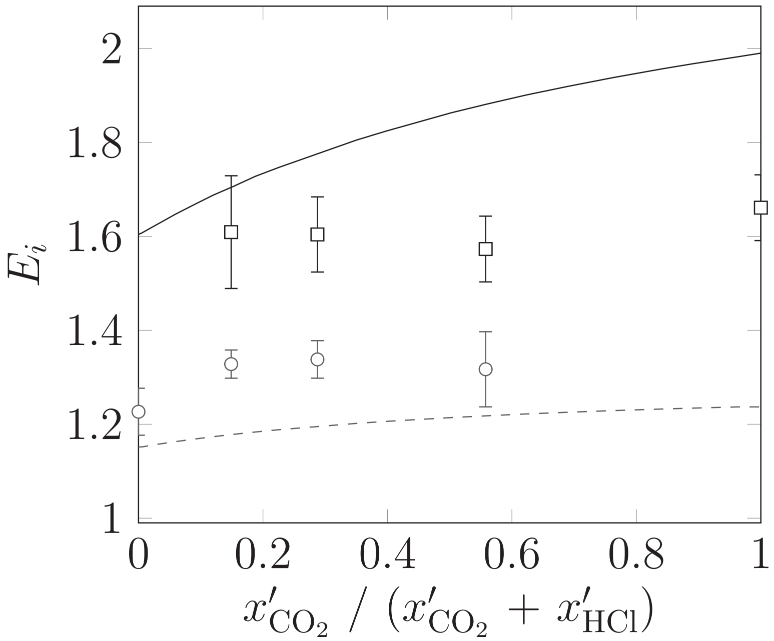

Figure 18: Interfacial enrichment of CO_2 (□, —) and HCl (○, - - -) as a function of the composition of the liquid phase in ternary mixtures with toluene in VLE at T = 353 K and p = 4.9 MPa. Symbols are the present MD simulations results and lines are DGT + PC-SAFT results.

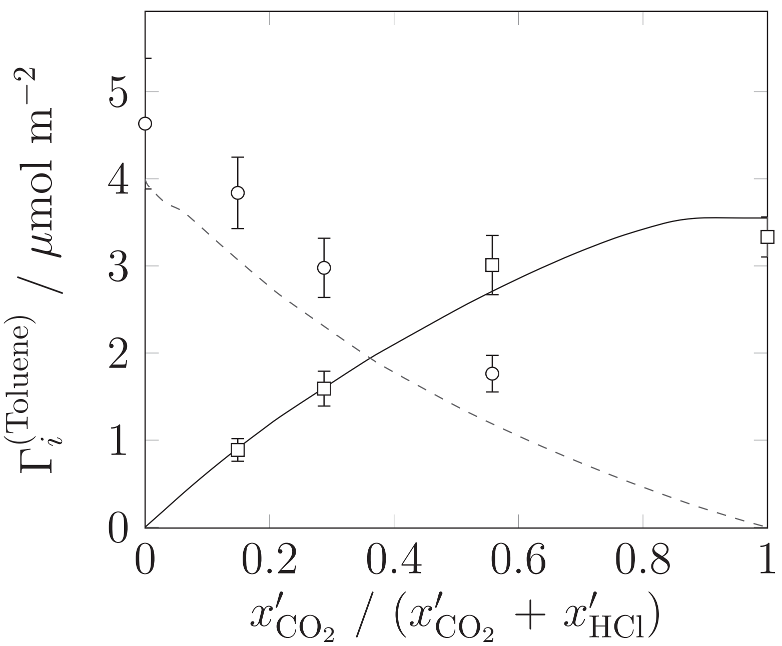

Figure 19: Relative adsorption of CO_2 (□, ––) and HCl (○, - - -) at the interface, defined such that $\Gamma_{\mathrm{Toluene}} = 0$, as a function of the composition of the liquid phase in the ternary systems with toluene in VLE at T = 353 K and p = 4.9 MPa. Symbols are the present MD simulations results and lines are DGT + PC-SAFT results.

Table 1: Literature overview of experimental data of the binary mixtures investigated in the present work.

Author	T / K		p / MPa	
	min	max	min	max
Toluene + CO_2 (VLE)				
Chen and Fang [9]	333	-	1.00	9.40
Yang et al [10]	308	343	3.21	9.46
Tochigi et al. [11]	323	333	1.08	9.89
Park et al. [12]	333	393	3.98	15.4
Naidoo et al. [13]	283	391	0.41	12.1
Morris and Donohue [14]	353	413	0.26	13.2
Muhlbauer and Raal [15]	352	-	0.88	11.0
Kim et al. [16]	353	393	0.52	6.45
Walther et al. [17]	352	389	6.15	14.3
Toluene + CO_2 (Henry's law constant)				
Horvath et al. [104]	298	300		
Field [105]	283	313		
Fink and Hershey [81]	308	353		
Waeterling et al. [106]	476	-		
Sebastian et al. [107]	393	542		
Nig and Robinson [108]	311	477		
Zhang et al. [109]	275	328		
Piskovsky and Lakomy [110]	198	293		
Shenderei et al. [111]	228	248		
Toluene + HCl (Henry's law constant)				
Ahmed et al. [100]	195	293		
Bell [101]	293	-		
O'Brian and Bobalek [102]	293	-		
Brown and Brady [103]	195	-		
HCl + CO_2 (VLE)				
Ansdall [18]	273	320	2.82	9.34
Dorsman [19]	293	324	4.24	6.17

Table 2: Binary interaction parameters ξ for the molecular models.

Mixture	ξ	Ref.
Toluene + CO_2	0.950	This work
Toluene + HCl	0.981	[3]
CO_2 + HCl	0.970	This work

Table 3: Pure component PC-SAFT and DGT parameters.

Compound	m	σ	ϵ/k_B	$10^4\kappa^{AB}$	$\epsilon^{AB}/k_\mathrm{B}$	n_A	n_P	n_E	Ref.	$10^{20}\kappa^\mathrm{DGT}$	Ref.
-		Å	K		K				-	J m^5 mol^{-2}	-
Toluene	2.8149	3.7169	285.69	-	-	0	0	0	[4]	31.010	This work
CO$_2$	2.0729	2.7852	169.21	-	-	0	0	0	[4]	2.5435	[97]
HCl	1.5888	2.9567	206.91	5.7172	1039.8	0	1	1	This work	2.0131	This work

Table 4: Binary interaction parameters k_{ij} for the PC-SAFT models for the mixtures considered in the present work.

Mixture	k_{ij}
Toluene + CO_2	0.12
Toluene + HCl	0.03
CO_2 + HCl	0.05

Table 5: MD simulation results for the vapor-liquid equilibrium of the pure components. The number in parentheses indicates the statistical uncertainty in the last decimal digit.

T K	p^{S} MPa	ρ' mol l^{-1}	ρ'' mol l^{-1}	γ mN m^{-1}
Toluene				
278	0.0011(6)	9.590(5)	0.0005(1)	34.1(7)
333	0.015(5)	9.008(3)	0.0057(14)	27.4(8)
353	0.034(4)	8.791(1)	0.0121(9)	24.3(9)
411	0.198(11)	8.117(4)	0.064(4)	17.4(7)
473	0.743(42)	7.288(1)	0.236(15)	10.6(3)
534	2.070(58)	6.187(2)	0.704(20)	4.4(3)
CO_2				
220	0.552(39)	26.345(9)	0.332(13)	19.1(6)
240	1.226(46)	24.591(20)	0.719(40)	13.6(6)
260	2.373(49)	22.563(29)	1.425(39)	8.7(6)
280	4.18(14)	20.048(53)	2.73(15)	4.3(5)
290	5.33(11)	18.307(64)	3.78(14)	2.4(4)
HCl				
180	0.058(15)	33.294(7)	0.043(13)	29.5(4)
210	0.304(19)	31.016(3)	0.191(15)	22.8(6)
240	0.961(53)	28.508(8)	0.569(28)	15.7(12)
270	2.427(31)	25.538(16)	1.470(25)	9.2(6)
290	3.986(91)	23.055(29)	2.566(94)	5.2(5)
300	5.01(52)	21.515(68)	3.428(75)	3.3(5)

Table 6: MD simulation results for Henry's law constant of CO_2 and HCl in toluene. The number in parentheses indicates the statistical uncertainty in the last decimal digit.

T K	$H_{\mathrm{CO_2,Toluene}}$ MPa	$H_{\mathrm{HCl,Toluene}}$ MPa
245	2.4(26)	0.5(15)
295	7.29(86)	2.11(58)
345	15.05(35)	5.52(27)
395	21.95(24)	10.25(19)
445	26.87(17)	14.76(13)
395	28.07(15)	17.93(11)
445	23.64(33)	17.61(25)

Table 7: MD simulation results for the vapor-liquid equilibrium of the binary mixtures of Toluene and CO_2. The number in parentheses indicates the statistical uncertainty in the last decimal digit.

T K	p MPa	$x'_{\mathrm{CO_2}}$ mol mol^{-1}	$x''_{\mathrm{CO_2}}$ mol mol^{-1}	ρ' mol l^{-1}	ρ'' mol l^{-1}	γ mN m^{-1}	$\Gamma^{(\mathrm{Toluene})}_{\mathrm{CO_2}}$ μmol m^{-2}	$E_{\mathrm{CO_2}}$ -
333	0.19(1)	0.012(1)	0.902(8)	9.070(8)	0.07(1)	26.3(18)	0.2(0)	2.79(46)
	1.08(4)	0.080(1)	0.984(4)	9.442(12)	0.41(2)	23.9(3)	1.0(0)	2.22(8)
	2.47(14)	0.199(4)	0.991(3)	10.15(3)	0.98(4)	20.3(6)	2.3(3)	1.84(10)
	3.52(17)	0.269(6)	0.991(4)	10.60(3)	1.47(7)	17.6(4)	3.2(4)	1.80(12)
	4.75(45)	0.365(7)	0.992(2)	11.28(5)	2.09(18)	14.2(7)	4.4(5)	1.63(9)
	6.26(15)	0.463(5)	0.992(2)	12.05(4)	3.01(11)	10.5(12)	6.1(5)	1.53(4)
	7.26(22)	0.542(3)	0.991(2)	12.73(17)	3.74(19)	7.6(9)	7.0(4)	1.39(4)
	8.14(13)	0.621(7)	0.990(4)	13.38(3)	4.52(16)	6.0(5)	8.0(11)	1.27(3)
353	0.23(3)	0.012(1)	0.967(4)	8.850(12)	0.08(1)	24.2(16)	0.2(0)	2.53(30)
	1.34(9)	0.080(3)	0.983(6)	9.203(11)	0.48(4)	22.1(5)	0.9(1)	2.06(21)
	3.11(36)	0.198(7)	0.985(2)	9.860(5)	1.12(9)	18.1(16)	2.0(4)	1.74(15)
	4.34(9)	0.264(2)	0.987(1)	10.28(1)	1.71(3)	15.4(9)	3.1(1)	1.72(5)
	4.90(12)	0.299(5)	0.985(3)	10.50(6)	1.98(12)	14.4(7)	3.3(2)	1.66(7)
	5.90(10)	0.360(3)	0.985(4)	10.89(4)	2.47(3)	12.7(8)	3.8(4)	1.55(9)
	7.87(20)	0.454(7)	0.985(3)	11.57(6)	3.60(15)	8.4(10)	5.2(4)	1.47(6)
	9.11(19)	0.538(6)	0.982(5)	12.17(4)	4.49(14)	6.3(4)	5.9(5)	1.33(4)
	10.3(2)	0.612(6)	0.979(3)	12.73(3)	5.44(14)	4.2(6)	6.4(10)	1.22(2)

Table 8: MD simulation results for the vapor-liquid equilibrium of the binary mixtures of Toluene and HCl. The number in parentheses indicates the statistical uncertainty in the last decimal digit.

T	p	x'_{HCl}	x''_{HCl}	ρ'	ρ''	γ	$\Gamma^{(\mathrm{Toluene})}_{\mathrm{HCl}}$	E_{HCl}
K	MPa	mol mol^{-1}	mol mol^{-1}	mol l^{-1}	mol l^{-1}	mN m^{-1}	μmol m^{-2}	-
333	0.18(1)	0.019(1)	0.965(7)	9.217(7)	0.068(2)	26.1(26)	0.3(0)	2.08(27)
	1.13(2)	0.213(6)	0.998(5)	10.85(2)	0.441(17)	21.4(18)	2.1(6)	1.67(21)
	2.47(3)	0.375(3)	0.998(3)	12.36(1)	1.313(21)	18.2(14)	3.7(5)	1.48(7)
	4.47(4)	0.517(3)	0.996(3)	13.43(1)	2.073(21)	14.1(10)	5.9(3)	1.31(5)
	6.26(8)	0.693(8)	0.995(4)	15.75(5)	3.377(88)	8.2(11)	9.0(12)	1.16(5)
	6.35(7)	0.708(5)	0.995(3)	15.95(4)	3.456(75)	8.0(13)	9.4(7)	1.09(3)
353	0.20(1)	0.019(1)	0.935(12)	9.037(8)	0.072(1)	23.1(28)	0.3(0)	1.99(24)
	1.34(3)	0.214(2)	0.998(1)	10.69(2)	0.488(12)	19.3(10)	1.9(5)	1.53(31)
	3.51(4)	0.377(2)	0.993(6)	11.76(2)	1.625(15)	16.4(14)	3.4(4)	1.37(10)
	4.90(5)	0.464(2)	0.992(8)	12.80(1)	2.158(14)	14.5(22)	4.6(8)	1.35(6)
	5.78(4)	0.510(1)	0.990(8)	12.92(1)	2.588(25)	11.8(23)	5.5(5)	1.30(5)
	8.11(10)	0.687(1)	0.988(2)	14.94(2)	4.291(69)	6.3(6)	7.5(8)	1.11(4)
	8.18(5)	0.699(2)	0.989(5)	15.09(2)	4.300(47)	6.0(3)	7.5(7)	1.09(3)

Table 9: MD simulation results for the vapor-liquid equilibrium of the ternary mixtures of Toluene + CO_2 + HCl at 353 K. The number in parentheses indicates the statistical uncertainty in the last digit.

p MPa	$x'_{\mathrm{CO_2}}$ mol mol^{-1}	x'_{HCl} mol mol^{-1}	$x''_{\mathrm{CO_2}}$ mol mol^{-1}	x''_{HCl} mol mol^{-1}	ρ' mol l^{-1}	ρ'' mol l^{-1}	γ mN m^{-1}	$\Gamma^{(\mathrm{Toluene})}_{\mathrm{CO_2}}$ μmol m^{-2}	$\Gamma^{(\mathrm{Toluene})}_{\mathrm{HCl}}$ μmol m^{-2}	$E_{\mathrm{CO_2}}$ -	E_{HCl} -
4.91(21)	0.066(3)	0.378(7)	0.202(14)	0.790(14)	12.25(8)	2.02(10)	14.8(8)	0.9(1)	3.8(4)	1.61(12)	1.33(3)
4.89(24)	0.121(5)	0.301(8)	0.362(12)	0.630(12)	12.01(12)	1.94(11)	16.0(19)	1.6(2)	3.0(3)	1.58(7)	1.34(4)
4.93(21)	0.217(9)	0.172(7)	0.627(18)	0.367(20)	11.87(8)	2.02(8)	15.9(6)	3.0(3)	1.8(2)	1.60(8)	1.32(8)

Supplementary information to
Interfacial and Bulk Properties of Vapor-Liquid Equilibria in the System Toluene + Hydrogen Chloride + Carbon Dioxide by Molecular Simulation and Density Gradient Theory + PC-SAFT

Stephan Werth[a], Maximilian Kohns[a], Kai Langenbach[1,a], Manfred Heilig[b], Martin Horsch[a], Hans Hasse[a]

[a] *University of Kaiserslautern, Laboratory of Engineering Thermodynamics, Erwin-Schrödinger Str. 44, D-67663 Kaiserslautern, Germany*
[b] *GCP Chemical and Process Engineering, BASF SE, D-67056 Ludwigshafen, Germany*

---

1. Vapor-liquid equilibrium of Carbon dioxide + Hydrogen chloride

At 333 and 353 K, the subsystem carbon dioxide + hydrogen chloride is supercritical, so that no VLE exists. Therefore, simulations at 290 K were performed and the binary interaction parameter ξ was adjusted to fit the azeotropic pressure [1], which they do well. The temperature of 290 K is still quite close to the critical temperature of both fluids. Figure 1 shows the phase diagram of the system hydrogen chloride + carbon dioxide at that temperature. The experimental data are interpolated to 290 K from isopleths using Antoine fits. The simulation results agree fairly well with experimental data [1, 2] considering the vicinity to the critical point. The compositions in the vapor and the liquid are very close to each other over the entire pressure range, and the azeotropic behavior is well described by MD simulations as well as the PC-SAFT equation of state.

[Figure 1 about here.]

Figure 2 shows the interfacial tension of carbon dioxide + hydrogen chloride mixtures at 290 K as a function of the mole fraction of CO_2 in the liquid phase. The magnitude of the interfacial tension is much smaller than in the toluene-containing systems due to the vicinity to the critical point. The interfacial tension of pure carbon dioxide and hydrogen chloride is experimentally available and in good agreement with the simulation data. The results from the molecular simulation show an almost linear decrease of the interfacial tension from the value of pure hydrogen chloride to the value of pure carbon dioxide. The results from DGT + PC-SAFT show nonlinear behavior and a minimum of the interfacial tension close to the azeotropic point.

[Figure 2 about here.]

The system carbon dioxide + hydrogen chloride shows azeotropic behavior, cf. Figure 1. Due to the fact that both phases have a similar composition over the entire pressure range, no considerable adsorption at the interface occurs. This is confirmed by the present data.

The numerical values of the molecular simulation results for the VLE of the binary system are given in Table 1.

[Table 1 about here.]

2. Relative adsorption based on the Gibbs adsorption equation

As defined by Gibbs [3], the relative adsorption of CO_2 at the interface in VLE with toluene at constant temperature is given by

$$\Gamma_{\mathrm{CO_2}}^{(\mathrm{Toluene})} = -\left.\frac{\mathrm{d}\gamma}{\mathrm{d}\mu_{\mathrm{CO_2}}}\right|_T , \qquad (1)$$

where $\mu_{\mathrm{CO_2}}$ is the chemical potential of CO_2. In Figure 3 the relative adsorption of CO_2 at the vapor-liquid interface in VLE with toluene at 353 K is shown. Over a large concentration range, the relative adsorption calculation based on the Gibbs adsorption equation, cf. equation (1), and the calculation based on the density profile are equal. Only for concentrations close to the critical point, the calculated values of the MD simulations based on the Gibbs adsorption equation are smaller than the values obtained from the density profile of the MD simulations.

[Figure 3 about here.]

References

[1] G. Ansdell. *Proc. Roy. Soc. London*, 34:113–119, 1882.

[2] C. Dorsman. *Isothermen van Mengsels van Zoutzuur en Koolzuur*. PhD thesis, Univ. van Amsterdam, 1908.

[3] J. W. Gibbs. *The Scientific Papers of J. W. Gibbs.* Dover Publications, 1961.

[4] G. N. Muratov and V. P. Skripov. *Teplofiz. Vys. Temp.*, 20:596–598, 1982.

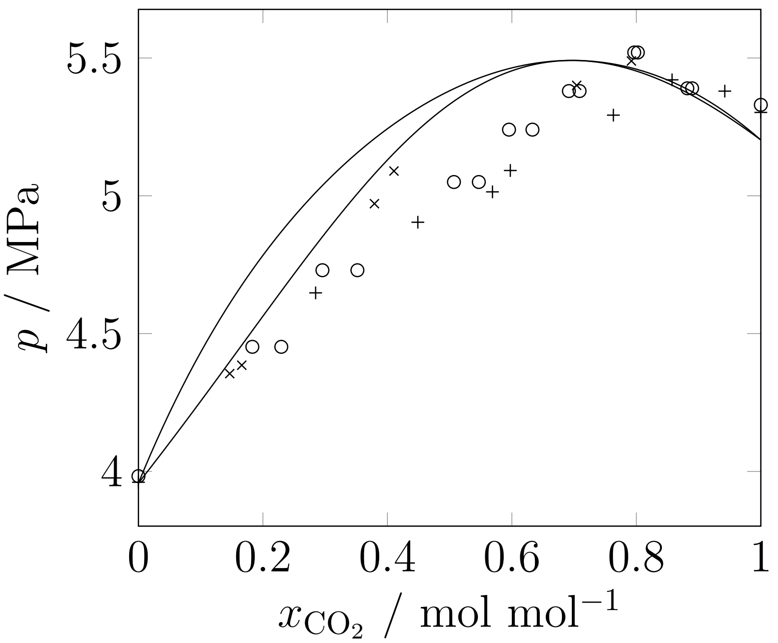

Figure 1: Vapor-liquid equilibrium of binary mixtures of carbon dioxide and hydrogen chloride at 290 K. Symbols are the present MD simulation results, lines are PC-SAFT results, and crosses [1] and pluses [2] are experimental data for the liquid phase extracted from isopleths via Antoine fits.

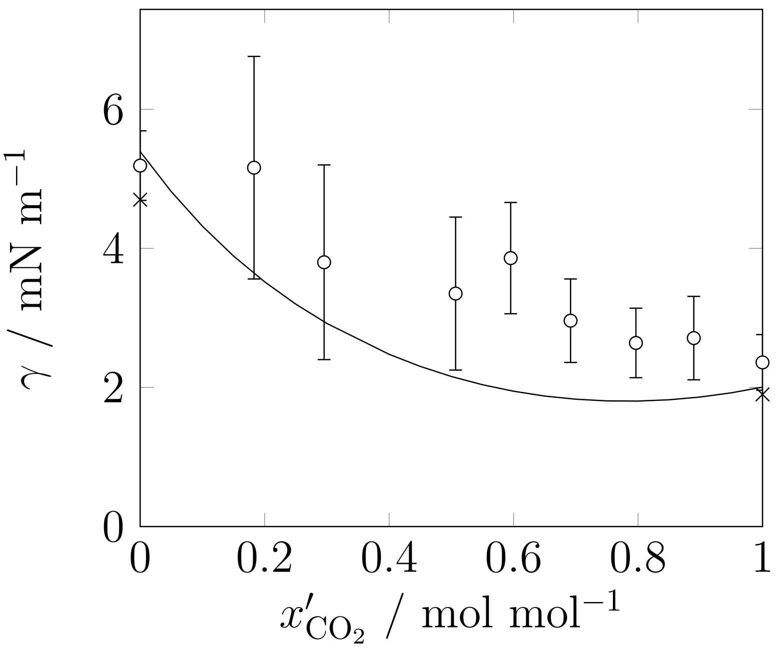

Figure 2: Interfacial tension of binary mixtures of carbon dioxide and hydrogen chloride at 290 K as a function of the mole fraction of CO_2 in the liquid phase. Symbols are the present MD simulation results, lines are DGT + PC-SAFT results and crosses are experimental results for the pure components [4].

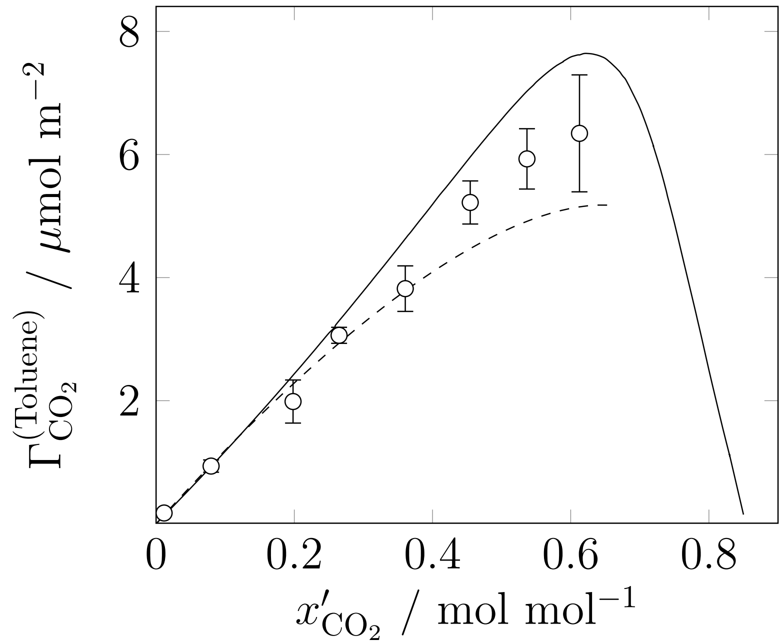

Figure 3: Relative adsorption of CO_2 at the interface defined such that $\Gamma_{\mathrm{Toluene}} = 0$, as a function of the mole fraction of CO_2 in the liquid phase with toluene in VLE for 353 K (○, —). The symbols are MD simulation results and the solid line are DGT + PC-SAFT results based on the density profiles. The dashed line represents the calculation based on the Gibbs adsorption equation, cf. equation (1).

Table 1: Molecular simulation results for the vapor-liquid equilibrium of the binary mixtures of HCl and CO_2 at 290 K. The number in parentheses indicates the statistical uncertainty in the last decimal digit.

p MPa	$x'_{\mathrm{CO_2}}$ mol mol^{-1}	$x''_{\mathrm{CO_2}}$ mol mol^{-1}	ρ' mol l^{-1}	ρ'' mol l^{-1}	γ mN m^{-1}
4.45(4)	0.183(1)	0.230(9)	22.20(3)	2.77(8)	5.1(16)
4.73(9)	0.296(1)	0.352(19)	21.62(2)	2.95(7)	3.8(14)
5.05(9)	0.507(2)	0.547(26)	20.61(4)	3.24(28)	3.4(11)
5.24(4)	0.595(3)	0.633(19)	20.25(1)	3.15(21)	3.9(8)
5.38(8)	0.692(5)	0.709(22)	19.75(3)	3.46(48)	3.0(11)
5.52(14)	0.797(2)	0.802(14)	19.39(2)	3.65(8)	2.6(5)
5.39(4)	0.890(2)	0.882(5)	18.85(8)	3.34(32)	2.7(6)